# POINT CLOUDS AND THERMAL DATA FUSION FOR AUTOMATED GBXML-BASED BUILDING GEOMETRY MODEL GENERATION

A Dissertation
Presented to
The Academic Faculty

by

Chao Wang

In Partial Fulfillment
of the Requirements for the Degree
Doctor of Philosophy in the
School of Civil and Environmental Engineering

Georgia Institute of Technology
August, 2014

# POINT CLOUDS AND THERMAL DATA FUSION FOR AUTOMATED GBXML-BASED BUILDING GEOMETRY MODEL GENERATION

Approved by:


Dr. Yong K. Cho, Advisor
School of Civil and Environmental Engineering
*Georgia Institute of Technology*

Prof. Godfried Augenbroe
School of Architecture
*Georgia Institute of Technology*

Dr. Lawrence F. Kahn
School of Civil and Environmental Engineering
*Georgia Institute of Technology*

Dr. T. Russell Gentry
School of Architecture
*Georgia Institute of Technology*

Dr. Patricio Antonio Vela
School of Electrical and Computer Engineering
*Georgia Institute of Technology*


Date Approved: Jun 27th, 2014

Dedicated to my family for their unwavering support

# ACKNOWLEDGEMENTS

The achievements of my past five years have not been possible without the help of numerous professors, colleagues, friends, and family members. First and foremost, I would like to express my utmost gratitude to my doctoral advisor, Dr. Yong K. Cho, for the opportunities for research, teaching, and service he afforded me throughout my time at both the Georgia Institute of Technology and the University of Nebraska-Lincoln. This dissertation and my research work would not have been possible without his support and guidance. His passion for research in construction robotics and automation is infectious and motivating to all those around him. He's given me full support as I overcame all the obstacles to complete this research. I would also like to thank other members of my doctoral committee, including Dr. Lawrence F. Kahn, Prof. Godfried Augenbroe, Dr. T. Russell Gentry, Dr. Patricio Antonio Vela, Dr. Terence Foster, Dr. Hongrong Li, and Dr. Hassan Farhat, for their time and advice.

Much of the success during my doctoral study can be attributed to my fellow lab colleagues, including Thaddaeus Bode, Diego Martinez, Heejung Im, Koudous Kabassi, Ziqing Zhuang, Mengmeng Gai, Qinghua Xu, Keke Zheng, Jeewoong Park, Yihai Fang, Kyungki Kim, Sijie Zhang, Nipesh Pradhananga, and Arif Allama. I thank them for helping collect data and offer words of encouragement, and their support was critical to my accomplishments. I look forward to continuing professional relationships as well as friendships with these great people.

Lastly, I would like to dedicate this dissertation to my parents, wife, and all of my friends for their unconditional love ad support throughout my whole life.

# TABLE OF CONTENTS

# LIST OF TABLES

# LIST OF FIGURES

## SUMMARY

Existing residential and small commercial buildings now represent the greatest opportunity to improve building energy efficiency. Building energy simulation analysis is becoming increasingly important because the analysis results can assist the decision makers to make decisions on improving building energy efficiency and reducing environmental impacts. However, manually measuring as-is conditions of building envelops including geometry and thermal value is still a labor-intensive, costly, and slow process. Thus, the primary objective of this research was to automatically collect and extract the as-is geometry and thermal data of the building envelope components and create a gbXML-based building geometry model.

In the proposed methodology, a rapid and low-cost data collection hardware system was designed by integrating 3D laser scanners and an infrared (IR) camera. Secondly, several algorithms were created to automatically recognize various components of building envelope as objects from collected raw data. The extracted 3D semantic geometric model was then automatically saved as an industry standard file format for data interoperability. The feasibility of the proposed method was validated through three case studies.

The contributions of this research include 1) a customized low-cost hybrid data collection system development to fuse various data into a thermal point cloud; 2) an automatic method of extracting building envelope components and its geometry data to generate gbXML-based building geometry model. The broader impacts of this research are that it could offer a new way to collect as is building data without impeding

occupants' daily life, and provide an easier way for laypeople to understand the energy performance of their buildings via 3D thermal point cloud visualization.

# CHAPTER 1

# INTRODUCTION

## 1.1 Background

Energy efficiency has been a significant issue for the whole world since the energy crisis in the late 1970's (Maldague 2001). In the United States, buildings sector currently accounts for approximate 41% of the primary energy usage (Brass 2007; U.S. DOE 2011; EIA 2009), as shown in Figure 1.1, commercial buildings and residential buildings consume 19% and 22% of the total U.S. energy consumption. The U.S. Department of Energy's Build America Program (NREL 2008) set a goal of reducing the average energy use in housing by 40% to 70%. President Obama also launched the Better Building Challenge which asks leading organizations to commit to reducing the energy use of their buildings by 20% by the year 2020. In buildings sector, around 95% of buildings (over 120 million) are existing residential buildings, which represent the single largest contributor to U.S. energy consumption and greenhouse gas emissions (over 50%). Since existing residential buildings are the single largest contributor to the U.S. energy consumption, conducting retrofits on the existing residential buildings, especially on those aged buildings, will have the greatest potential to improve building energy efficiency and reduce environmental impacts and the total energy consumption in the U.S.

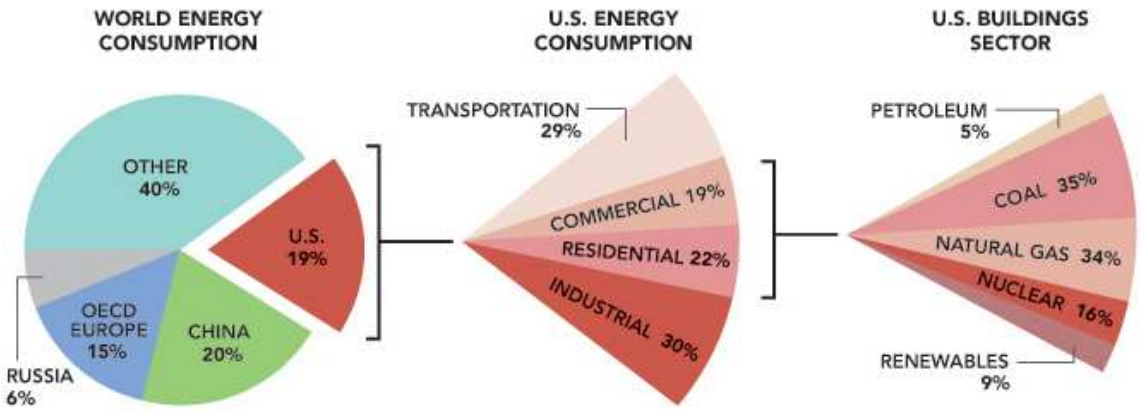


**Figure 1.1: Energy consumption by sector (U.S. DOE 2011)**

To help retrofits of existing residential buildings, a detailed building energy performance assessment is desired for the building stakeholders for their decision making process. Building energy performance assessment requires information about buildings, such as their geometry, material, internal loads, and weather conditions (Azhar and Brown 2009). It is important to obtain accurate as-is data about the buildings because this information directly affects the building energy performance assessment results. For the existing buildings, sometimes this as-is data are on record, but it may be inaccurate due to the building's renovation, insulation aging, and home owner's lack of technical knowledge. Among all the desired as-is data, collecting as-is geometry data about the building envelope components is a more labor-intensive, costly, and time-consuming process.

Recently, with the development of the as-is modeling technique, 3D as-is point cloud can be collected by using laser scanner or photogrammetry technique. Point cloud is composed of millions of individual points in which each one has a 3D relative coordinate information. Tang et al. (2010) reviewed the current related techniques for

automatic reconstruction of as-is building information models from point clouds. Figure 1.2 shows an example of 3D as-is point cloud collected from a 3D laser scanner, and the color was rendered based on the distance to the scan location. The 3D building envelope can be well visualized in the collected point cloud. However, the collected point cloud is not useful for building energy analysis until as-is building data being extracted. Current as-is building data extraction is mostly done through manual processes, and few research efforts have been done to automate this manual process.

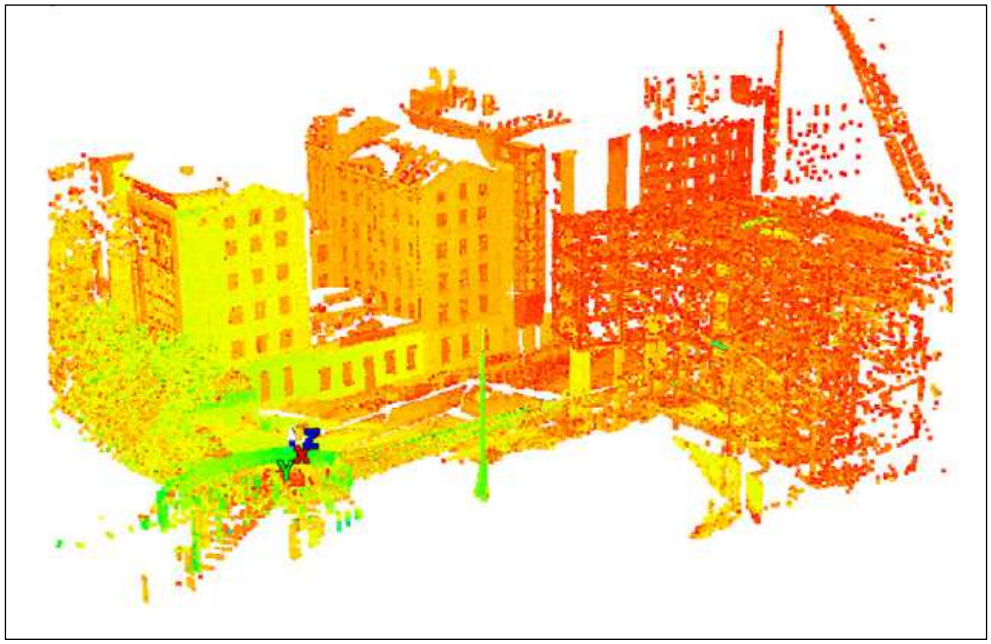

**Figure 1.2: An example of point cloud data collected from a building (Tang et al. 2010)**

## 1.2 Research Hypothesis

The hypothesis of this research was that the integration of as-is point cloud data with as-is infrared (IR) thermography data can improve the automated 3D semantic

geometric modeling process. With the abovementioned research hypothesis, several research questions were proposed in the followings,

***Research Question 1:*** *How can the as-is point cloud and thermal data be non-invasively collected, fused and visualized?*

***Research Question 2:*** *How can the semantic data be automatically extracted from the collected raw data?*

***Research Question 3:*** *How can the extracted semantic data be stored in terms of data interoperability?*

## 1.3 Research Objectives and Scopes

The ***primary objective*** of this research was to automatically collect and extract the as-is geometry and thermal data of the building envelope components and auto-generate a gbXML-based building geometry model.

The specific research objectives were:

**Objective #1:** Design and identify a hybrid data collection and processing system which non-invasively collects and fuses as-is point cloud and thermal information from a building envelope.

**Objective #2:** Create algorithms which can automatically recognize various components of building envelope as objects from collected raw data. Evaluate the precision, recall, and accuracy of the proposed algorithms.

**Objective #3:** Identify a method which can automatically convert extracted building geometry and thermal data to a file format that is interoperable with the energy simulation tool.

In this research, the test subjects were residential houses or small commercial buildings, and it was assumed that the completely registered point clouds of buildings for testing proposed framework and algorithms were available using all existing advanced data collection technologies (e.g., Unmanned Aerial Vehicle (UAV), photogrammetry, videogrammetry, etc.) in addition to the hybrid data collection system developed in this research. The scope of this research included hybrid data collection system design, data fusion and semantic data extraction, gbXML geometry modeling and data interoperability of extracted semantic data. An energy simulation tool (Autodesk Ecotect Analysis 2011) was used to test the semantic gbXML data interoperability, and whether the semantic data can be successfully imported or not was evaluated. Neither energy simulation analyses (e.g., energy annual consumption, thermal & light simulations) nor comparisons with existing energy auditing methods were part of the research scope.

## 1.4 Dissertation Organization

This research aimed to investigate a method of fusing point clouds with thermal data for gbXML-based building geometry model generation. Table 1 provided a brief description of the contents of each chapter.

**Table 1.1: Title and description of each dissertation chapter**

| Chapter | Description |
|---|---|
| 1) Introduction | This chapter introduces background, problem statement, research hypothesis, research objectives and scope. |
| 2) Literature Reviews | This chapter reviews the closely related research conducted by other researchers on the technology and development of as-is thermal building modeling. |
| 3) Overview of The Proposed Methodology | A brief overview and the framework of the proposed methodology are presented. |
| 4) Non-invasive As-Is Thermal Modeling | The main objective of this chapter is to develop a hybrid data collection system that can non-invasively collect and fuse 3D point cloud and temperature data from existing buildings. |
| 5) Automated gbXML-based Building Geometry Model Generation | The primary objective of this chapter is to provide a preliminary solution that automatically and rapidly extracts building envelope components of existing buildings from point cloud data that can be further utilized for gbXML-based geometry model generation. |
| 6) Conclusions | This chapter summarizes the research findings and concludes the dissertation. Future research extensions and opportunities of this research are discussed as well as limitations. |

# CHAPTER 2

# LITERATURE REVIEWS

The object of this chapter is to review the closely related research conducted by other researchers on the technology and development of as-is thermal building modeling. In order to develop this study, three categories of the existing literature have been reviewed, including: 1) As-is point cloud creation methods; 2) As-is thermal modeling methods; and 3) Object recognition from point clouds.

## 2.1 State-of-the-art Point Cloud Collection Methods

A point cloud is a set of data points in which each point has its relative coordinates, and often is intended to represent the external surface of an object. It may be created by photogrammetric method or 3D laser scanner. A point cloud can be post-processed to render real-size objects or environment by registering all individual scans onto the same coordinates. Point cloud registration is defined as registering multiple point clouds scanned from different viewpoints into one common coordinate system. Recent studies have been made on how the as-is point cloud can be created to represent existing buildings.

### *2.1.1. Stereo vision and photogrammetry*

A stereo imaging system comprises multiple passive 2D imaging sensors (cameras) with fixed or regularly calibrated imaging parameters. Imaging parameters include the interior orientation parameters of a camera depicting the projection and imaging geometry, and the exterior orientation parameters depicting the relative position and orientation relationships among multiple cameras (Linder 2003). With the stereo imageries and these parameters, a photogrammetric algorithm can extract and match feature points across images composed of overlapping regions, and reconstruct 3D measurements on these regions (Linder 2003). Several researchers have explored the application of such systems to construction progress monitoring and management (Brilakis et al. 2010; Dai and Lu 2010). While stating the limitations of requiring interior and exterior parameters to be known, some studies have explored approaches capable of automatically estimating the interior and exterior parameters of cameras for 3D reconstruction based on unordered photographs with limited interior parameters known (Golparvar-Fard et al. 2009b). Digital videogrammetry (Figure 2.1) has also been demonstrated as being advantageous in some situations; however, it is currently restricted to fixed camera positions (Brilakis et al. 2010).

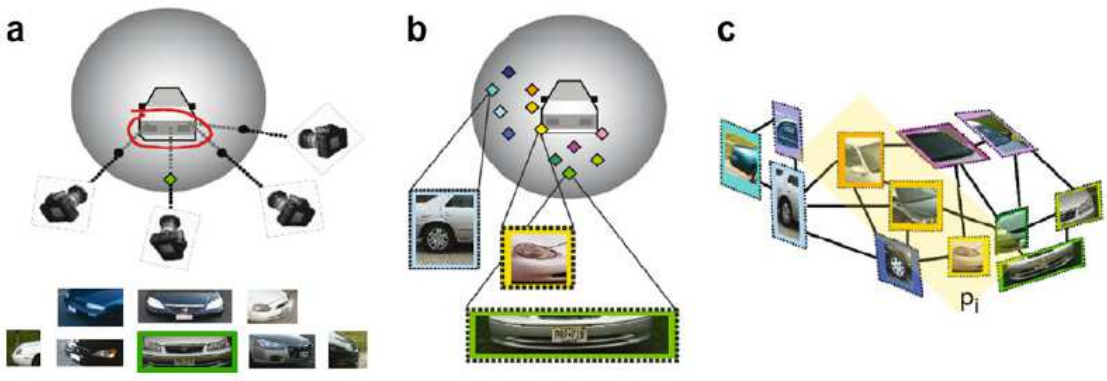


**Figure 2.1: Representation for modeling process using digital videogrammetry (Brilakis et al. 2010)**

Photographs provide large amounts of information about the progress of construction. The information provided may be automatically processed and converted (Navon 2007; Brilakis and Soibelman 2008, Golparvar-Fard and Peña-Mora 2007; Wu and Kim 2004; Abeid et al. 2003). Furthermore, compared to other data collection techniques, photographs do not hinder efficient project management processes by requiring significant data collection efforts (Golparvar-Fard et al. 2009a; Bhatla et al. 2012). Golparvar-Fard et al. (2009b) introduced an image-based as-built modeling technique based on computing from the images themselves, the photographer's locations and orientations, and a sparse 3D geometric representation of the as-built scene using daily progress photographs (Figure 2.2). The major advantages of photogrammetric systems include fast data collection rates (tens to hundreds of 1024 × 1024 pixel frames per second), and acquisition of rich color and textural information of workspace objects for appearance based object recognition. Published research results show that most of these systems can be used to model a workspace in a well-controlled environment such as structured indoor manufacturing. However, this method has a number of limitations:

Different lighting and weather conditions make it difficult to use time-lapse photography for performing consistent image analysis at occluded and dynamic site conditions (Golparver-Fard et al. 2011; Golparvar-Fard et al. 2009a, Golparvar-Fard et al. 2009b, Bohn and Teizer 2010). Further, the geometry of the area will be overlooked if common features from multiple images cannot be found. If there has been significant construction progress and photographs were not taken or some objects were moved (e.g., equipment or scaffoldings) during that period, it would be challenging to find common feature points in photographs. In addition, manually taken photos cannot completely avoid spatial information discontinuity (Golparvar-Fard et al. 2011; Golparvar-Fard et al. 2009a). Bhatla et al. have also shown that the technology in its present state is not suitable for modeling infrastructure projects (Bhatla et al. 2012).

**Figure 2.2: An example of the reconstructed sparse scene of as-built site point cloud data by processing site images (Golparvar-Frad et al. 2009b)**

*2.1.2. Laser scanners*

A laser scanning system is composed of a photon source that emits a continuous laser signal or a series of laser pulses, mechanical components for rotating the photon

source vertically and horizontally to scan the scene with a laser, and a timing system for deriving the time-of-flight and determining ranges. A scanning system sequentially collects 3D points while rotating the photon source, thereby generating 3D points column by column to form a panoramic range image of the scene (Farid and Sammut 2012). State-of-the-art laser scanning technology provides approximately 4 mm distance accuracy and 6 mm positional accuracy at up to 50 m distance for a single measurement. In construction applications, the accuracy of laser-scanned data depends on a number of factors beyond the underlying sensor accuracy. These factors include object dimension, surface orientation, surface reflectivity, and environmental lighting and temperature conditions (Akinci et al. 2006).

Compared to photography, laser scanners facilitate wide-range measurements at higher resolutions and accuracies, and are generally not limited by ambient conditions during operation (Anil et al. 2013). Laser scanning can also better holistically address all of the listed inefficiencies associated with the current practice of progress monitoring through rapid and detailed geometric data collections than other 3D remote sensing technologies (Golparvar-Fard 2011). In the domains of construction and facility management, researchers have conducted various studies investigating the issues related to utilizing laser scanners for a wide range of purposes, including fast workspace modeling (Cho et al. 2002; Kwon et al. 2004), real-time safety management on site (Bhatla et al. 2012), construction progress monitoring (Bosche and Haas 2008; Bosche and Haas 2007; El-Omari and Moselhi 2008; Reboli et al. 2008, Xiong et al. 2013), defect detection (Akinci et al. 2006; Gordon and Akinci 2005), as-built modeling (Cheok et al. 2000; Heinz et al. 2001; Kim et al. 2005; Anil et al. 2011; Adan and Huber 2011),

deflection assessments of bridges (Gordon et al. 2004; Jaselski et al. 2005; Jaselskis et al. 2006; Xiong et al. 2013; Tang and Akinci 2008; Tang et al. 2007; Tang et al. 2011), and pavement thickness assessments (Jaselskis et al. 2006).

Depending on the types of signals emitted from the photon source and the timing mechanism for deriving distances, two types of laser scanning systems exist on the market. Time-of-Flight (TOF) systems use photon sources emitting discrete laser signals, and directly measure the time difference between sending and receiving the signals for deriving the distances. Phase-Shift systems emit continuous modulated laser signals with certain light wave shapes, and use the phase-shift between the sent and received light wave for deriving the travel time of the laser and determining the distances. Both systems have their advantages and disadvantages for real-time construction applications. Two main issues that influence such applications are the data collection rate and the range of the scanner. Generally, a scanner with fast data collection rate is preferred for real-time applications, but a long range scanner can cover a large area at one station as long as the occlusions are not serious on jobsites, so that engineers can save time for moving the scanner on jobsites.

*TOF scanning systems:* the principle behind a TOF system is that the laser is pulsed several thousand times per second (up to 50,000 with some recently released models) for range detections.

Once the scanner has calculated the distance, both the horizontal angle and the vertical angle are measured to yield the 3D point. In this case, the distance and coordinates of the reflecting object are determined by the following Equation 2.1:

$$\rho = \frac{1}{2} c\Delta t,$$

$$\begin{bmatrix} x \\ y \\ z \end{bmatrix} = \begin{bmatrix} \rho \cos \beta \cos \alpha \\ \rho \cos \beta \sin \alpha \\ \rho \sin \beta \end{bmatrix} \qquad \text{Equation 2.1}$$

Where, ρ=distance, c=light speed, and Δt=time interval, α=horizontal angle, and β=vertical angle.

Typical TOF scanners have a data collection rate of thousands to tens of thousands points per second. One scan will last between a few minutes to several hours, depending on the frequency of the photon source and the spatial resolution of the collected data. Most terrestrial TOF scanners have long data collection ranges of hundreds of meters. Some TOF scanners can reach more than 1km for monitoring extra-large infrastructure systems, such as dams or bridges (Alba et al. 2006). For all TOF systems, the reflectivity of targeted objects influences the data quality so that the actual range with data qualities meeting most domain requirements vary with the reflectivity of objects of interest.

**Figure 2.3: An Example of TOF laser scanners (Leica Scan Station C10) (Leica 2014)**

Figure 2.3 shows a Leica Scan Station C10 which is an example of TOF laser scanners. The major limitation of TOF scanning systems is their relatively low data collection rates. Even with the fastest TOF scanner on the market today, a panoramic scan with a spatial resolution of 2 cm at 100 m needs about two and half hours to be completed based on the authors' experimental results. This fact indicates that for capturing any objects as small as 2 cm at 100m, the data collection time for the whole scene would be inacceptable for real-time monitoring of most construction operations. It is necessary to develop methods for better utilizing the data collection capability to obtain all needed data under time constraints.

*Phase-shift scanning systems*: the phase-shift scanning systems use a different distance measuring principle to achieve a much higher data collection rate compared with TOF systems. Unlike a TOF scanner which pulses the laser, a phase-shift scanner uses a modulated laser light that is always on. The photon source emits a continuous laser wave with a modulated frequency and wavelength. This continuous laser signal then bounces off objects, and returns to the photon receiver of the scanner with a shift in phase when compared against the leaving signal. This phase-shift can be measured for deriving the light travelling time (Equation 2.2) and then the distance. Once the distance is calculated, the azimuth and elevation angle measurements are applied to produce the 3D coordinates (Kemeny and Turner 2008).

$$\text{Time of Flight} = \text{Phase Shift} / (2\pi * \text{Modulation Frequency}),$$

Equation 2.2


**Figure 2.4: An Example of Phase-shift scanning systems (FARO 2014)**

Phase-shift systems can capture hundreds of thousands to millions of 3D points

per second, which is about ten times faster than most TOF scanning systems (Tang et al 2009; FARO 2010). As shown in Figure 2.4, FARO Focus 3D is an example of Phase-shift scanning system. The best working range for most phase-shift scanners is less than 100 m. Beyond that range, range ambiguity issues (Stone et al 2004), mixed pixels (Tang et al 2009), and other technical difficulties not sufficiently resolved yet would result in noisy data, so that valid and accurate 3D measurements would be few. In addition, the impact of low reflectivity on phase-shift data was observed to be more significant than that of TOF data according to the experiences of the authors. For improving the data qualities of phase-shift systems, multiple modulation frequencies are being explored, but the improved results have not yet achieved the same level of data quality as TOF systems (Kemeny and Turner 2008).

The limitations of phase-shift systems include the relatively limited ranges and the data quality issues caused by special reflectivity of dark or specular objects, and spatial discontinuities. Many objects on the jobsites, such as steel, glasses, and aluminum frames, would not be captured with high precision and details, since most data points on them are noisy and should be removed by noise filtering algorithms. For cluttered jobsites, noisy data at object boundaries can cause inaccurate measurement of object dimensions and may mislead decisions about construction operations (Tang et al 2009). As a result, even with high data collection rates, obtaining all needed information from phase-shift data still requires improvements of the overall data quality.

*Flash LADAR Systems:* also called 3D range cameras, are also based on the time-of-flight measurement principle using laser. Instead of sequentially collecting 3D points while scanning, a Flash LADAR flood-illuminates the scene with laser flashes, and

captures a range image for each flash (also known as a flash frame). The estimated absolute positioning accuracy with one pixel of a recently released Flash LADAR is +/- 1.5 cm with up to 50 frames per second (FPS) under well-controlled indoor lighting conditions. That flash LADAR system's non-ambiguity measurement ranges from 0.8 to 5 meters (Mesa Imaging 2010). Compared to laser scanning systems, a flash LADAR is smaller, less expensive, and forms 3D images in real time. The disadvantages include a relatively limited field of view compared with the panoramic field of view of a laser scanning system, and lower accuracy and spatial resolution. In addition, flash LADAR systems are designed mainly for indoor applications since the associated noise level makes it impossible to work in direct sunlight, where light shielding may be needed to suppress background illuminations (Mesa Imaging 2010; Cho and Martinez 2009; Anderson et al 2005). Figure 2.5 shows an example of Flash LADAR.


**Figure 2.5: An Example of Flash LADAR (SR-3000) (Hegde ad Ye)**

*Self-Positioning Handheld Laser Scanner:* Self-positioning handheld laser scanners are being used by many industries, such as aerospace, manufacturing,

multimedia, and medicine, as they provide an easy and fast way to acquire 3D geometries (Smithm 2011). These mobile scanners utilize photogrammetric processing, automatic calibration, and automatic referencing for self-positioning. Several companies market such self-positioning handheld laser scanners, including Z Corporation, NDI, Creaform, Nikon, Hexagon, Romer, Leica, and Steinbichler (DirectIndustry 2010). This type of scanner uses the subject part being scanned to establish its spatial reference. The self-positioning mechanism of these scanners eliminates the need for fixed-position tripods, bulky mechanical arms or external positioning devices causing accessibility problems. Uniquely object-referenced, they also allow the target object to move during scanning, and allow the viewing of a real-time image of the surface being scanned. These scanners generate one continuous scan rather than multiple scans from multiple positions, eliminating post-processing time for registering multi-scans.

In a series of studies conducted by the authors, Z Corporation's ZScanner 700™ was tested to explore its usability for construction applications. The results show that this scanner's accuracy can achieve 40µm (microns), and it is possible to detect 50 µm changes in surface height from the collected point clouds. This scanner can capture 18,000-25,000 3D measurements per second. To achieve higher self-positioning accuracy and overall data quality, it optionally uses reflective targets, which can be quickly and randomly applied to the surfaces of the objects to be scanned and/or the area adjacent to these surfaces. During the scanning process, the scanner locates and captures the reflective positioning targets by a stereo camera, which estimates 3D positions of these targets in real time. These positions are calculated in reference to the scanner's line laser

and then recorded in the scanner. As the targets randomly applied on the object create unique perspective-dependent patterns recognizable by the scanner, the scanner will be able to position itself in the same way that GPS devices use known satellites to establish their position on Earth (Z Corporation 2011).


**Figure 2.6: Example of incomplete scan due to a complex feature (e.g., ear)**

Due to its portability and very high accuracy, self-positioning handheld scanners can be used in reverse engineering in structural component design, quality control for prefabricated materials, building damage inspection, rapid prototyping, and education. The real-time and continuous scanning mechanism enables such scanners to capture geometries of moving objects, which are important for real-time construction operation monitoring. The major limitation of such scanners is that most of them have very short measurement ranges (< 1 m). In addition, if the scanned objects are not visible from any one of the two cameras of its stereo camera system, it cannot derive complex surface geometries well due to occlusions. In such cases, the stereo camera system of the scanner can just see the targeted object with one “eye”, resulting in an incomplete shape. An example of this problem is shown in Figure 2.6. The range limitation and the necessity of

a clear stereo view of the targeted objects seriously limit the applicability of these scanners on clutter construction jobsites with complex geometries and occlusion conditions. Table 2.1 below summarizes the advantages and disadvantages of various data collection and processing techniques reviewed in this subsection.

**Table 2.1: Summary of advantages and disadvantages of various 3D data collection and processing techniques**

| Category | Advantages | Disadvantages |
|---|---|---|
| **Stereo Imaging and Photogrammetric Systems** | • Real-time capturing color and textural information<br>• Semi-real-time generation of sparse 3D measurements | • Sensitive to lighting conditions<br>• Challenging for acquiring detailed geometries of surface lacking feature points<br>• Challenging for reliably reconstructing 3D geometries of surfaces with repetitive patterns |
| **TOF Laser Scanning Systems** | • Long range for covering large open space<br>• High accuracy for individual points | • Relatively low data collection rate, making it impractical for real-time workspace monitoring |
| **Phase-Shift Laser Scanning Systems** | • Fast data collection rate for capturing detailed geometries in minutes within short ranges (tens of meters) | • Relatively low data qualities compared with TOF data, especially on dark, specular surfaces, and at spatial discontinuities<br>• Relatively short range compared with TOF systems |
| **Flash LADAR Systems** | • Capturing 3D snapshots of a scene with moving objects with high frequencies (e.g., 50 FPS)<br>• Small sizes<br>• Less expensive | • Limited field of view<br>• Relatively low positioning accuracy<br>• Relatively low spatial resolution of each scan (3D frame)<br>• Relatively more sensitive to outdoor lighting conditions |
| **Self-Positioning Handheld Laser Scanner** | • Very high positioning accuracies (µm-level)<br>• Portability<br>• Capturing moving objects with continuous scanning and self-positioning mechanisms, eliminating data registration needs | • Very short data collection ranges (< 1m)<br>• Require the targeted objects to be visible in both cameras of the stereo camera system embedded in the scanner, causing challenges for modeling complex geometries with a lot of occlusions |

### *2.1.3 Point cloud data structure*

The point clouds collected from various devices can be categorized as either organized or unorganized. An organized point cloud has a data structure that is similar to an image or a matrix, and each point of the point cloud has its index in rows and columns. Such point clouds include data collected from stereo cameras or time-of-flight cameras. The advantage of the organized point cloud over the unorganized point cloud is that data processing is more efficient because the relationship between adjacent points or nearest neighbors is known. In unorganized point clouds, no data structure or point reference exists between points because of varied sizes, resolutions, densities, and point sequences. As a result, more time is usually consumed processing unorganized point cloud data.

## 2.2 As-is 3D Thermal Modeling Methods

Most commercial survey-level laser scanners enable an internal or external camera to capture digital images of the scanned scene and map image textures onto corresponding points in point clouds, assigning each point values for position (x, y, z) and color (R, G, B). Unlike applications using digital cameras, there have been few efforts to map thermal images taken from an IR camera onto point clouds, although the IR thermography technique has long been used as a non-invasive approach to diagnose buildings and infrastructure (Balaras and Argiriou 2001). This section discusses state-of-the-art 3D thermal model creation techniques for existing buildings. Generally, there are three classes of 3D thermal modeling approaches: 1) infrared (IR) image mapping to 3D models; 2) image fusion and matching by IR image and digital image; and 3) IR image mapping to 3D point clouds. The following subsections will introduce these three

categories of techniques, and discuss the remaining technical gaps in 3D thermal modeling for existing buildings.

### *2.2.1 Infrared Image Mapping to 3D Models*

Schreyer and Hoque (2009) presented a method to create thermography-textured 3D digital models of buildings using IR images and SketchUp. In this method, the 3D model of the building was created with SketchUp, and the IR images were attached to the surfaces of the models as texture (Figure 2.7). While this method shows very clear thermal color distribution on the 3D model surface, it has these limitations: 1) a 3D model does not represent an as-built (or, as-is) design; 2) it is difficult to correctly align the IR image with the model without calibrating an IR camera; and 3) the final model shows only relative color differences based on temperature ranges but does not provide numerical temperature information.

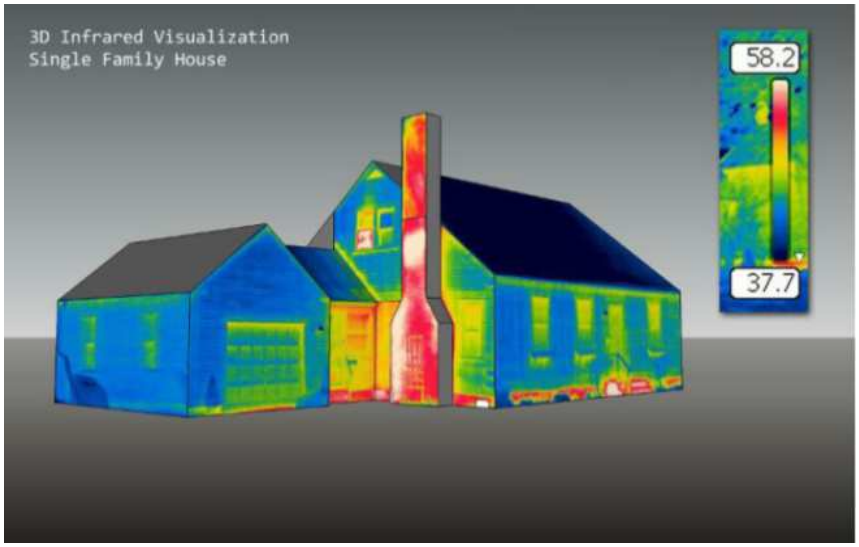


**Figure 2.7: Infrared Image Mapping to SketchUp Models (Schreyer and Hoque 2009)**

*2.2.2 Image Fusion and Matching by Infrared Image and Photogrammetry*

A thermographic 3D modeling method using image fusion and image matching techniques for building inspection was presented by Lagüela et al. (2011a). In this research, a digital image and an infrared image of the same building were collected individually and images were matched using the photogrammetry technique (Luhmann et al. 2006). Using the known measurements of two distances in the façade, the relative coordinates of four points were calculated. These values were needed for both image fusion and 3D modeling. While this technique provided good visual information to detect thermal differences in the building envelope, the temperature data captured by an IR camera were lost in the 3D thermal model. Because the thermal color of objects captured by an IR camera is determined relative to the surrounding environment, the same object (e.g., a wall) can be differently colored if the temperature range is different from another capture. In addition, the thermographic 3D modeling method requires that the images be captured with the camera parallel to the façade to obtain an orthothermogram of the façade, which limits the application of this method.

Another 3D thermal modeling system, Energy Performance Augmented Reality (EPAR), was introduced by Ham and Golparvar-Fard (2012). In this method, a handheld IR camera with a built-in digital camera was used to collect thermal and digital images simultaneously. Then a 3D thermal point cloud (Figur 2.7) was created by integrating visualization of both 2D thermal and digital images utilizing a 3D reconstruction technique called bundle adjustment or structure from motion (SFM) (Golparvar-Fard et al. 2009b; Borrmann et al. 2012b). This method would be useful for modeling plain indoor or confined spaces due to its good portability and mobility. Since the 2D image-

based 3D reconstruction approach needs to register hundreds of thermal and digital images, it requires up to six hours to create a complete 3D point cloud of a building (about 2.5M points; Ham and Golparvar-Fard 2012), and thus is useful only when modeling time is not pressing. As another limitation of this approach, the accuracy of the model is sensitive to lighting conditions, meaning a digital camera can collect building exterior data only in the daytime to reconstruct a 3D building model. However, thermal data need to be collected at night. Borrmann et al. (2012b) state that even diffuse sunlight on a cloudy day distorts the thermal measurements in a way that a meaningful analysis becomes impossible.

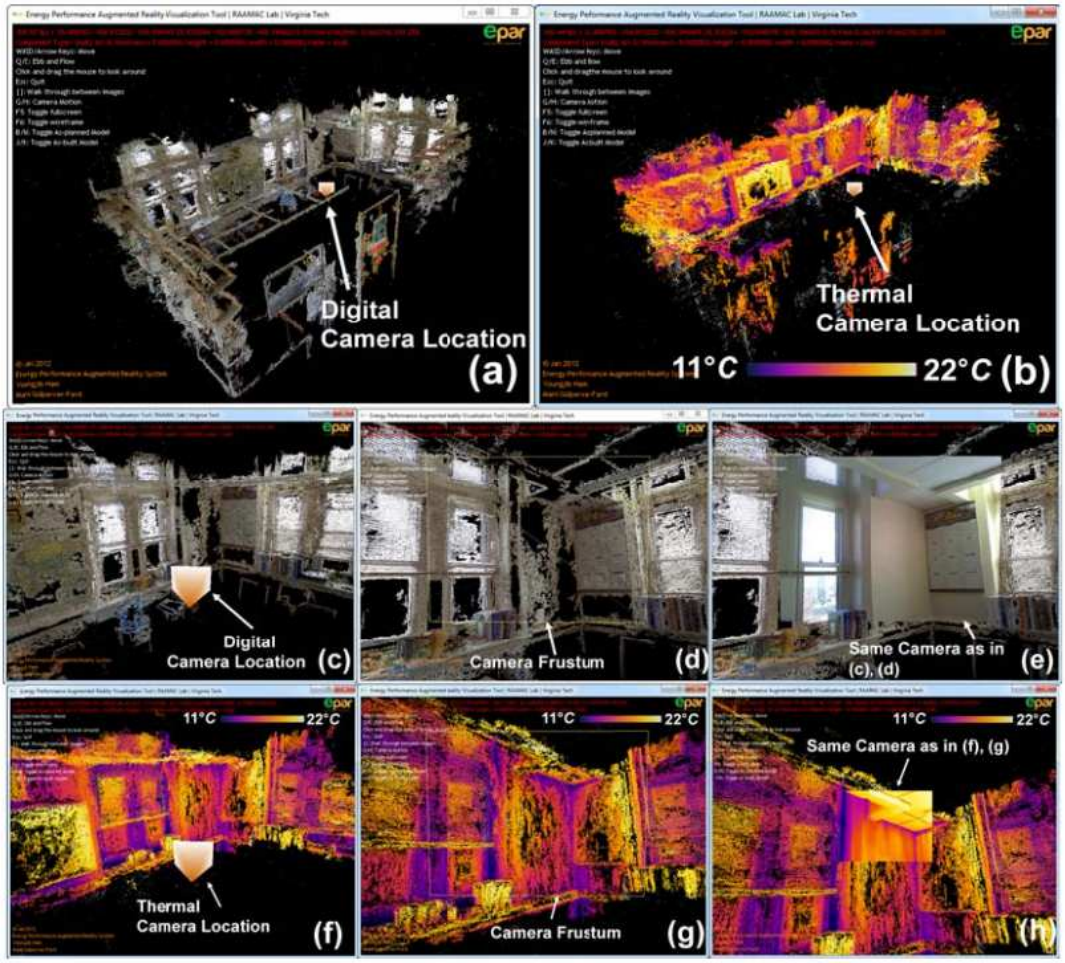


**Figure 2.8: 3D As-is building and thermal models (Ham and Golparvar-Fard 2012)**

*2.2.3 Infrared Image Mapping to 3D Point Cloud*

Alba et al. (2011) developed a bi-camera system consisting of IR camera, digital camera, and 3D laser scanner to acquire and integrate information for building diagnostic and restoration applications. The thermal data and the point clouds were fused by using control points that were measured manually by a digital camera and a laser scanner. A methodology for registering thermographies in point clouds was introduced by Lagüela et al. (2011b). An IR camera was calibrated to avoid image distortion before merging the thermographies into point clouds. The thermographies and point clouds were collected and registered separately, then merged together using common control points. This method could merge the temperature data with the corresponding points in the point clouds and reduce the image distortion. However, the captured temperature value is lost after it is merged with the point cloud; only the color difference based on a temperature range can be visualized. Also, the data collecting process is limited by two conditions: 1) the shooting direction of the IR camera has to be perpendicular to the facade; and 2) an overlap of 50% between consecutive thermographies is needed for image registration.

Against color-coded temperature data, thermal measurement with absolute temperature values in °C or °F provides more useful information for diagnosing building materials for their energy efficiency.

Borrmann et al. (2012b, 2012c) developed a 3D thermal modeling method using LIDAR and a low resolution IR camera (160 x120 pixels) mounted on a mobile robot Irma3D to expedite scanning and registration processes. The thermal data were matched to the corresponding point clouds, which were automatically registered using the 6D simultaneous localization and mapping (SLAM) technique (Borrmann et al. 2012a).

However, this system cannot collect data over 100 vertical degrees due to the limited camera field of view (360°*100°); thus a tall building needs to be scanned from a far distance, which would result in a low-resolution thermal 3D model. In the thermal mapping process, the thermal color other than temperature values was merged with the point cloud.

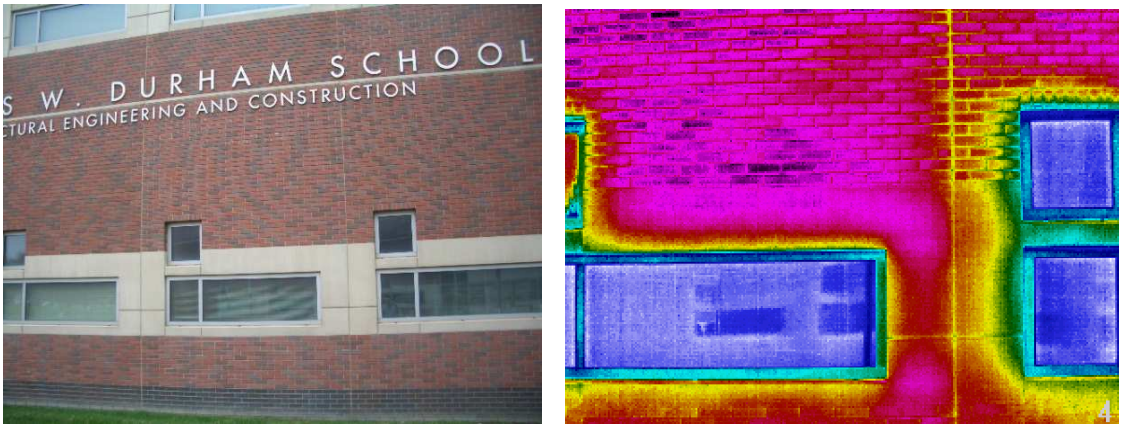


**Figure 2.9: A building image (left) and an IR thermal image of the building (right)**

From previous efforts, the research team developed an integration method which projects an infrared thermal image onto the point clouds by calculating distance, position and orientation between corresponding common points (Figure 2.9). Similar to Tsai and Lin's (2004) work, this approach merely merges the radiometric images to a 3D point-clouds model (Figure 2.10). While it is still good visual information to detect thermal differences of building materials, however, the captured temperature information by an infrared camera is lost in the 3D thermal model. The thermal color of captured objects is relatively determined by the surrounded environment in an IR camera. The same object (e.g., wall) can be differently colored if the temperature range is different from another

capture. Thus, the thermal measurement which provides absolute temperature values in °C or °F is more accurate information to diagnose building materials for their energy-efficiency.

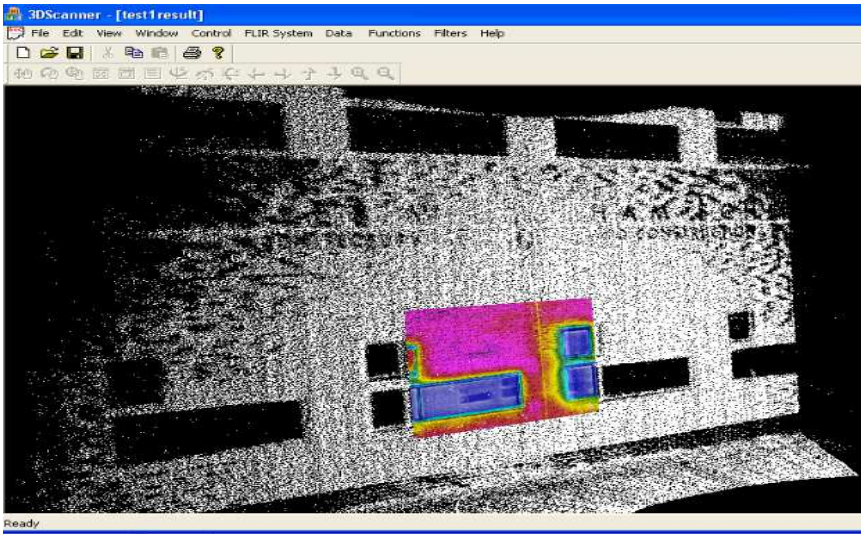


**Figure 2.10: IR image projected onto point clouds of the building (overlay)**

## 2.3 Object Recognition from Point Clouds

### *2.3.1 Existing Commercial Software*

Manually creating 3D model from point cloud is a labor-intensive and time-consuming process. Many commercial software programs or plug-ins have been developed to accelerate this manual process. For example, *Leica CloudWorx* (Leica 2014) is able to automatically create a pipe center line based on manually selected pipe, and then the pipe can be manually created following the center line; *Intergraph Smart 3D for Plants* (Intergraph 2014) can automatically model pipes after user identifying the scanned piping axis of symmetry; *Autodesk Plant 3D*® (Autodesk 2014) and *Kubit PointSense*

(Kubit 2014) *Plant* enable user for manually choosing two points from an image of a pipe, and the corresponding 3D point cloud between the two points can be automatically located and modeled; *Kubit PointSense Building* (Kubit 2014) can automatically generate 2D building plan (wall, floor, ceiling) from 3D laser scanner data, but with manual openings (window, door) creation; *AVEVA Laser Model Interface*$^{TM}$ (AVEVA Continual Progression 2014), *Trimble RealWorks* (Trimble 2014) and *ClearEdge3D* (ClearEdge3D, 2014) are designed to automatically create 3D model by manually segmenting the point cloud and choose the corresponding catalogs for each segment of point cloud. The abovementioned programs (see Figure 2.11) are all semi-automated, and most of them are for industrial application only. Therefore, there is a need for a method of fully automated model creation from point cloud, especially for building envelope modeling which is important to building energy simulation.

### *2.3.2 Recent Research Efforts towards Automated Object Recognition*

To recognize objects and extract useful object information from point clouds, object recognition techniques have frequently been applied in recent studies in the AEC/FM domain. Tang et al. introduced a method of extracting geometric information items of bridges from point cloud data, collected from a laser scanner, for bridge management (Tang and Akinci, 2012; Anil et al., 2013). Site laser scans have also been processed for 3D status visualization and construction progress monitoring. In (Bosche, 2010; Bosche et al., 2009), a new approach for automatic 3D CAD recognition and registration of steel structures was validated by processing the point cloud data of the steel structures. Advanced techniques and improvements in devices have resulted in

textured point cloud data becoming available. Son and Kim (2010) proposed a method for efficient, automated 3D structural component recognition and modeling from point cloud data with RGB color acquired from a stereo vision system. Point cloud data with RGB color can also be obtained by processing hundreds of photographs (Golparvar-Fard et al., 2009b) for construction performance monitoring and 4D as-is model creation.

Another set of approaches presented to assist building facility management and performance analysis include the proposal by Pu and Vosselman (2009). They proposed a knowledge based method for reconstructing building models from laser scanner data. In their method, they extract the features and the outline of the building and make the geometric model of the building based on several assumptions because only facades on the street side are scanned. Xiong et al. (2013) proposed a context-based modeling algorithm for creating semantic 3D as-is building models of the interior of buildings. Their context-based modeling algorithm was able to identify and model the main visible structural components of an indoor environment, but could not recognize components with irregular shapes that are frequently seen from the exterior of the building envelope. The components of the building envelope are essential for building performance analysis. As a result, rapid and efficient extraction of building envelope geometric information is a challenging emerging topic.

**Table 2.2: Literature review of the current as-is BIM recognition techniques**

| | Category | Advantages | Limitations |
|---|---|---|---|
| Commercial software programs | Leica CloudWorx (Leica Geosystems 2014) | ▪ Providing a point cloud processing plug-in capability for many of the most popular CAD systems<br>▪ Semi-automatic pipe center line creation<br>▪ Designed for various applications | ▪ Need manual point cloud segmentation and modeling object category selection |
| | Intergraph Smart 3D for Plants (Intergraph 2014) | ▪ Enabling user for comparison of as-designed model vs. as-is point cloud | ▪ Mainly for industrial application<br>▪ Need manually creating a pipe center line for pipe modeling |
| | Autodesk Plant 3D (Autodesk 2014) | ▪ More easily performing whole-project review.<br>▪ Customized standard equipment library<br>▪ Externally referencing or parametrically creating structural elements<br>▪ Combine 3D scanning, imaging and position data | ▪ Model spec-driven pipelines and components semi-automatically or manually<br>▪ Mainly for modeling pipe, equipment, and structure |
| | Kubit PointSense (Kubit 2014) | ▪ Semi-automatically generating 2D plans from 3D laser scanner data<br>▪ Designed for various applications<br>▪ Combine 3D scanning, imaging and position data | ▪ Two manually selected reference points needed for pipeline modeling<br>▪ Openings (windows, doors) need to be manually created in the 2D plans. |
| | AVEVA Laser Model Interface TM (AVEVA Continual Progression 2014) | ▪ Accurately positioning and clash checking new 3D design in situ within an existing installation | ▪ Need manual point cloud segmentation and modeling object category selection<br>▪ Limited for industrial application |
| | Trimble RealWorks (Trimble 2014) | ▪ Combine 3D scanning, imaging and position data<br>▪ Semi-automatically modeling pipes | ▪ Need manual point cloud segmentation and modeling object category selection |
| | ClearEdge3D (ClearEdge3D 2014) | ▪ Semi-automated feature extraction<br>▪ Deep integration with Revit, AutoCAD, PDMS and other platforms<br>▪ Designed for various applications | ▪ Need manually segmenting point cloud and selecting object category for object modeling |
| | **Academic research efforts (Pu and Vosselman 2009; Xiong et al. 2013; Díaz-Vilariño et al. 2013; Hlinks 2013)** | ▪ Automatically modeling for indoor environment<br>▪ Modeling regular shape | ▪ Difficult to accurately model curved shapes<br>▪ Incomplete building envelope components recognition |

## 2.4 Points of Departure

The literature review provided an overview of 1) As-is point cloud creation methods; 2) As-is thermal modeling methods; and 3) Object recognition from point clouds. For the existing research on automatic as-is thermal model creation of existing buildings, the remaining limitations of the current technologies are summarized as follows:

1) Lack of visual perception-based rapid and low-cost data collection system for as-is thermal modeling of existing buildings.
2) Lack of method that can automatically and rapidly extract building envelope geometry information from point clouds.

# CHAPTER 3

# OVERVIEW OF THE PROPOSED METHODOLOGY

The overall framework of the proposed methodology is shown in Figure 3.1. First, a hybrid 3D laser scanner system designed in this research simultaneously collected point clouds and temperature data from the envelope of existing buildings. Then temperature data were automatically fused with corresponding points during the data collection process. After registering all individual thermal point clouds, a building envelope recognition algorithm was applied to automatically create an as-is 3D geometric model. The as-is model can be imported into energy analysis software through being saved as an industry standard file format. Finally, the feasibility of the proposed method was validated through testing on two residential houses and a small bank building, and the performance of the proposed method was evaluated through calculating the precision, recall, and accuracy of the case studies.

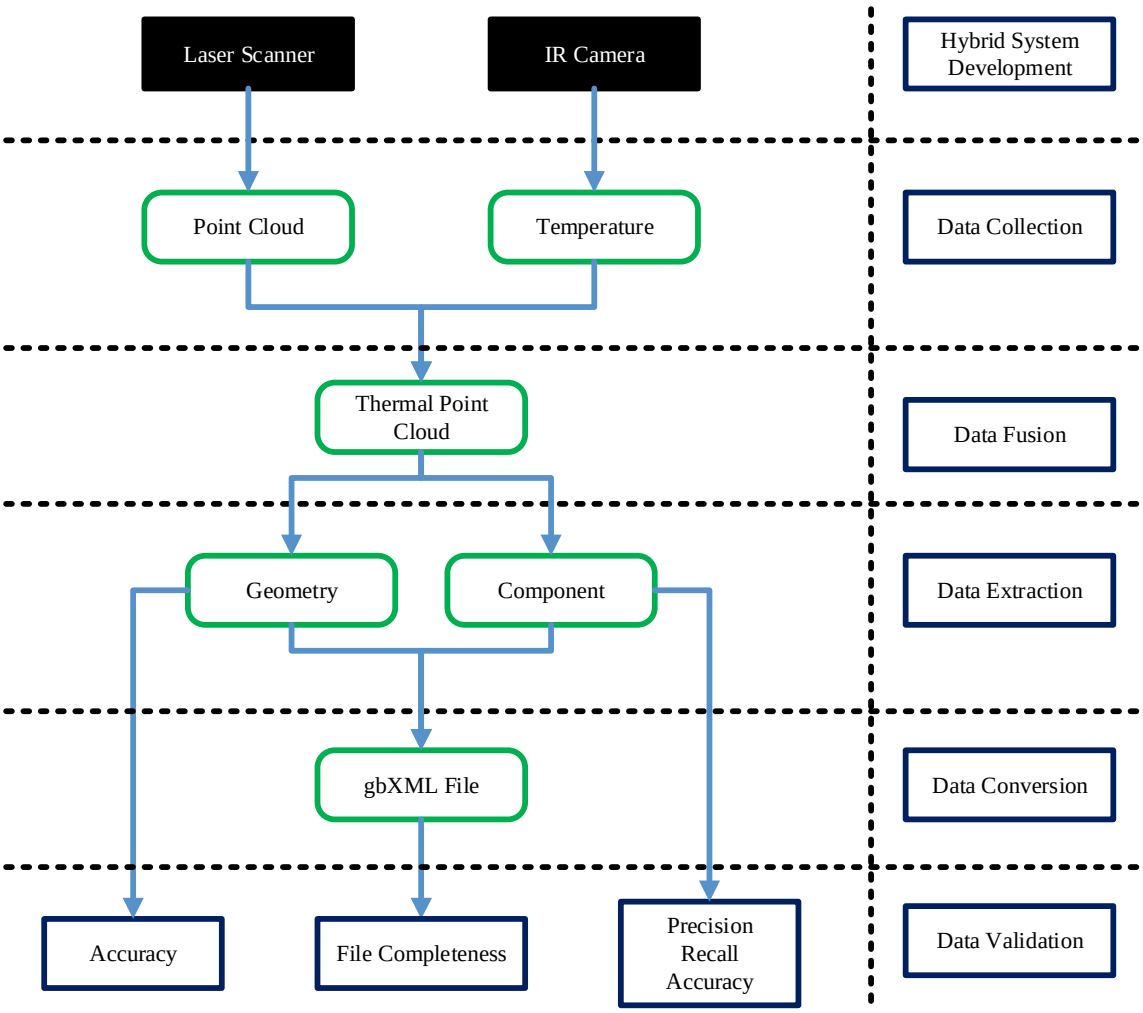


**Figure 3.1: Framework of the proposed methodology**

# CHAPTER 4

# NON-INVASIVE AS-IS BUILDING CONDITION DATA COLLECTION AND FUSION

Each aforementioned data collection method in Section 2.2 has advantages and disadvantages in terms of usability, lighting condition, modeling time, accuracy, and resolution. Through literature review, as-is 3D thermal modeling of existing building envelopes for energy performance analysis has not yet been fully recognized. Most especially, none of the current methods has realized the importance of thermal modeling of transparent windows, which are among the most important components affecting a building's heating and cooling loads. Thermal data on a window cannot be mapped to the point cloud because a laser scanner or a digital camera cannot recognize transparent glazing, resulting in a 3D thermal building model with many empty openings.

To address all the limitations mentioned above, a robotic hybrid thermal modeling approach was identified to directly fuse the temperature values, other than RGB values, with corresponding point cloud data to create a high-resolution 3D thermal model that overcomes the low-resolution characteristics of an IR camera. To generate complete thermal information about the building envelope, the missing points on glazing areas need to be virtually created.

The main objective of this chapter was to design a robotic hybrid data collection system that can non-invasively collect and fuse 3D point cloud and temperature data from existing buildings. In addition, two window detection algorithms are proposed to successfully fuse temperature data from transparent window glass, which cannot be

detected by a laser scanner or a digital camera. The following sections first present the design of the developed hybrid data collection system, and the 3D thermal modeling approach of the hybrid system is then discussed. Further, results of the two preliminary tests on a residential house and a commercial building are presented.

## 4.1 The Framework for Non-Invasive As-Is Building Condition Data Collection and Fusion

The overall framework of the proposed thermal modeling process for retrofit decision support is shown in Figure 4.1. First, a robotic hybrid data collection system designed in this study simultaneously collected point clouds and temperature data from the envelope of existing buildings. Temperature data were automatically fused with corresponding points during the data collection process. A noise filtering algorithm was then applied to each fused thermal point cloud to eliminate noisy geometric data which were defined as the points with fewer neighboring points than a preset threshold. After registering all individual thermal point clouds, a window detection algorithm was applied to create virtual thermal points on window glasses since the laser scanner is unable to collect geometric data from transparent objects. Finally, a 3D thermal point cloud was generated and visualized in a graphical user interface (GUI), and it was rendered with normalized thermal colors based on absolute temperature values. Further, the thermal point cloud can be imported into web-based geographical programs so that retrofit decision makers can have easy access to the as-is data and utilize it in their decision making process.

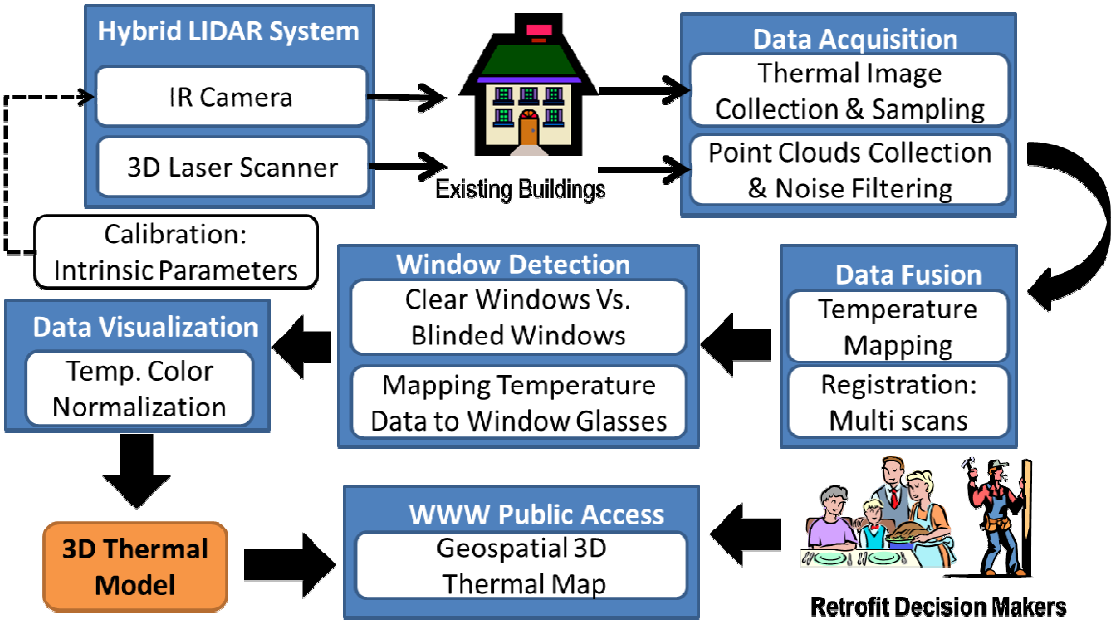


**Figure 4.1: Framework for 3D thermal modeling for retrofit decision support**

### 4.2 Robotic Hybrid Data Collection System

Thermography offers a rapid and cost-effective method of investigation that does not require any contact with surface materials or structure. Since it is a non-contact, non-destructive technique, thermography has been extensively utilized in the assessment of buildings, infrastructure, monuments, and ancient structures (Rao 2007; Ocaña et al. 2004; Rosina and Spodek 2003).

In this study, an innovative robotic hybrid system was developed, integrating a 3D LIDAR scanner and an IR camera (320 x 240 pixels), as shown in Figure 4.2. A GUI was developed using Visual C ++. The GUI controls the laser scanner and the IR camera, and visualizes the captured 3D model.

As a main sensor of the hybrid system, a light-weight 3D LIDAR was built consisting of a laser source, a spinning mirror, an encoder, and a pan and tilt unit (PTU).

Based on previous research (Cho and Martinez 2009; Cho et al. 2012), this lightweight 3D LIDAR would be more flexible in hardware control and software programming than a commercial laser scanner. Based on the current mounting configuration, multiple degree-of-freedom (DOF) kinematics was solved to obtain x-y-z coordinates from the LIDAR, and corresponding temperature data were obtained from the IR camera. The transformation matrices for the LIDAR and the IR camera share the first two frames and split into two different kinematics frames at the third matrix (Figure 4.3). This kinematics frame allows more optical sensors, such as digital video or still cameras, to be added.

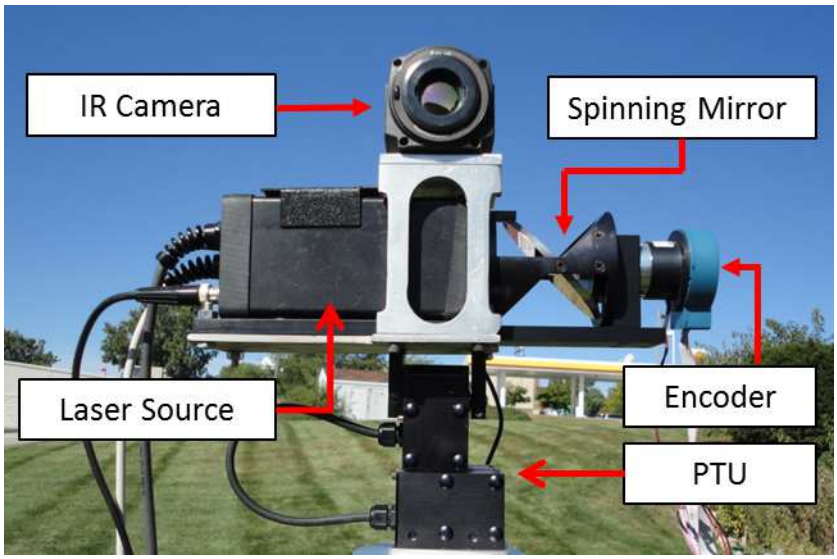


**Figure 4.2: Prototype I of the hybrid data collection system**

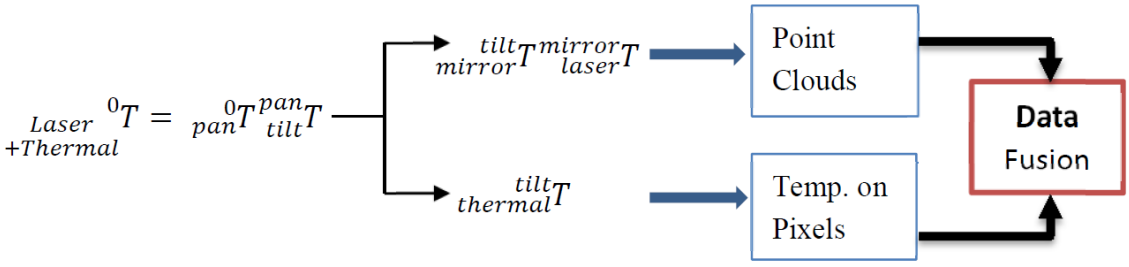


**Figure 4.3: Integrated kinematics frame for the hybrid data collection system**

## 4.3 3D Thermal Modeling Approach

### *4.3.1 IR Camera Calibration*

Camera calibration is an essential process in computer vision and 3D measurement applications because it corrects image distortion. Among types of image distortion, radial and tangential distortions are the worst (Ma et al. 2003). There are two categories of camera calibration variables: 1) intrinsic parameters that include focal length, principal point, skew coefficient, and distortion coefficients; and 2) extrinsic parameters that include rotation and translation matrix. To reduce distortions, the IR camera should be calibrated in advance to obtain the intrinsic parameters (Heikkila and Silven 1997; Bouguet 2010). Several camera calibration methods have been introduced elsewhere (Ma et al. 2003; Heikkila and Silven 1997; Bouguet 2010). In this study, Bouguet's (2010) camera calibration method was adopted. A black and white checkerboard was used as an object for testing the function. During the calibration process, the edge detection algorithms were applied to identify the structure of the checkerboard based on the different colors or gray scales; then the camera parameters could be accurately calculated (Drennan 2010). Unlike a normal digital camera, however, an IR camera cannot recognize different colors on the same material because the color or gray scale difference of the IR image can be distinguished only when a temperature difference on the image exists. Many researchers calibrate their IR cameras by taking thermographies on a calibration field consisting of a board with several light bulbs (e.g., LED lights) on it (Lagüela et al. 2011b; Ham and Golparvar-Fard 2012; Nüchter 2012).

To simplify the calibration process and lower the material cost, this study proposed the following IR camera calibration method: a cut-out checkerboard was made and placed in front of a human subject to make the checkered pattern recognizable in the IR images using heat radiation from a human body. The areas where the heat radiation was blocked by the checkerboard were rendered to a dark color in the IR images. Figure 4.4 shows the eight images that were taken as targets to be tested with the calibration program. The corner extraction process of the first image is demonstrated.

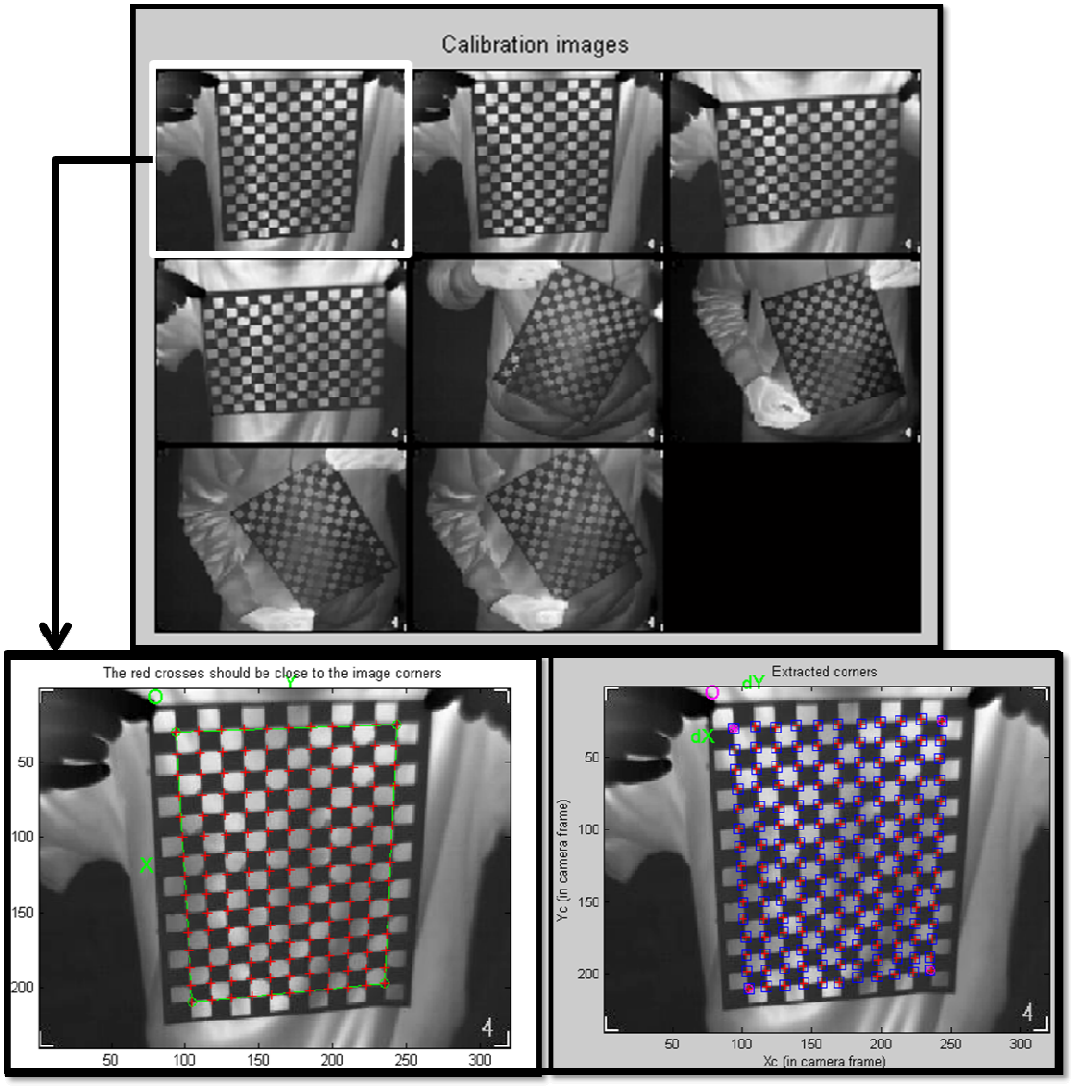


**Figure 4.4: IR camera calibration using heat radiation from the human body**

*4.3.2 Temperature Data Fusion*

The data fusion process is similar to texture mapping, a method for adding images as texture to the surfaces of the 3D models. The main difference in the proposed data fusion process is that the temperature data from each IR image pixel – instead of RGB pixel values – are directly extracted and assigned to points as non-graphic values. Thus, each point is considered an object containing different types of data, such as x-y-z coordinates, intensity, temperature, RGB, etc.

In order to map the temperature data to the point cloud correctly, the relationship between 2D temperature data and the 3D point cloud had to be built. First, the concept of perspective projection was introduced into the test, and a reference test was made to create a reference plane for the 3D projection. During the reference test, a 120cm×90cm rectangular object was used as a target, and both the laser rangefinder and the IR camera were placed parallel to the object. The distance between object and system was adjusted to make sure that the object completely filled the IR camera's view. As shown in Figure 8(a), the distance between object and camera is $f_{ref}$; $\theta$ *is* the IR camera view angle, and ($X_i$, $Y_i$, $Z_i$ ) represent the coordination of the point cloud in the system coordinate system. After calculations, several variables could be obtained as Equation 4.1:

$$f_{ref} = 166cm,\ \theta = 39.7^{\circ}, \qquad Pixel\ Unit = \frac{120}{320} = \frac{90}{240} = 0.375 \quad \text{(Equation 4.1)}$$

Having the reference plane, all the objects parallel to the system could be correctly mapped with temperature data according to Equation 4.2:

$$X_{pix} = \frac{X_i - \left(X_c - \frac{120 \times |Z_i|}{2 \times f_{ref}}\right)}{Pixel\ Unit \times \frac{|Z_i|}{f_{ref}}}, \qquad Y_{pix} = \frac{Y_i - \left(Y_c - \frac{120 \times |Z_i|}{2 \times f_{ref}}\right)}{Pixel\ Unit \times \frac{|Z_i|}{f_{ref}}} \qquad \text{(Equation 4.2)}$$

where $X_c$ and $Y_c$ are the coordinates of the point obtained when the laser is in its default position. $X_{pix}$ and $Y_{pix}$ are the coordinates of a pixel in the 2D IR image. Once the coordinates of the corresponding pixel were found, the temperature data was fused to the point in the 3D point cloud.

As shown in Figure 4.5(b), the camera was panned or tilted to obtain temperature data of another part of the point cloud. Under this circumstance, the reference plane is no longer parallel to the object. Due to the effect of the perspective projection, objects in the distance appear smaller than objects close by. As shown in Figure 4.5(c), if a simple interpolation were used and steps were equally spaced to compute pixel coordinates, a distorted image map would result. To avoid such a problem, the perspective correction method was used in this research. Perspective correction mapping interpolates after dividing by depth $Z_i$, then uses the interpolated reciprocal to recover the correct coordinate (Hill and Kelley 2006):

$$X_\alpha = \frac{(1-\alpha)\frac{X_a}{Z_a} + \alpha\frac{X_b}{Z_b}}{(1-\alpha)\frac{1}{Z_a} + \alpha\frac{1}{Z_b}}, \quad where\ 0 \le \alpha \le 1 \qquad \text{(Equation 4.3)}$$

When the camera is rotated, the area of the camera view varies based on the angle at which the camera is rotated. The coordinates of the edge points in the IR image can be calculated using Equation 4.4:

$$X_a = X_c + Z_c \tan\left(\alpha - \frac{\theta}{2}\right), X_b = X_c + Z_c \tan\left(\alpha + \frac{\theta}{2}\right) \qquad \text{(Equation 4.4)}$$

When the objects are not parallel to the camera, therefore, the temperature data can be mapped to the 3D point cloud using the following equation:

$$X_{pix} = \frac{X_i - X_a}{Pixel\ Unit \times \frac{|Z_i|}{f_{ref}} \times \frac{1}{X_a}}, Y_{pix} = \frac{Y_i - Y_a}{Pixel\ Unit \times \frac{|Z_i|}{f_{ref}} \times \frac{1}{X_a}} \quad \text{(Equation 4.5)}$$

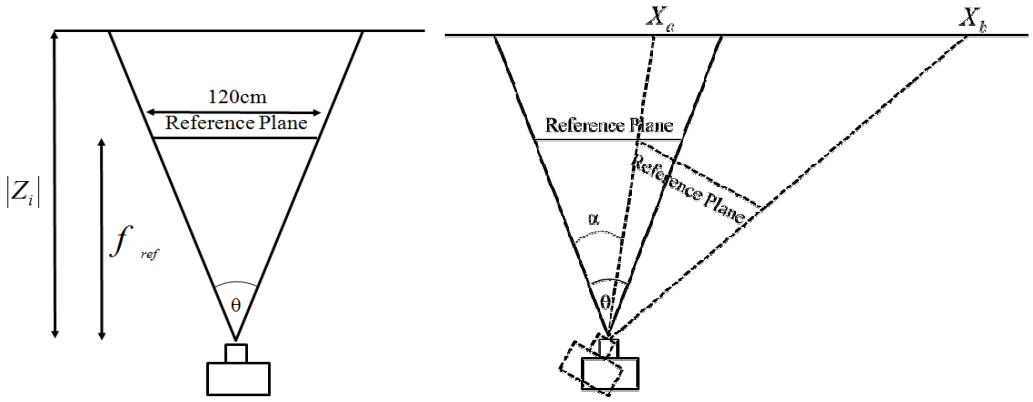


(a) (b)

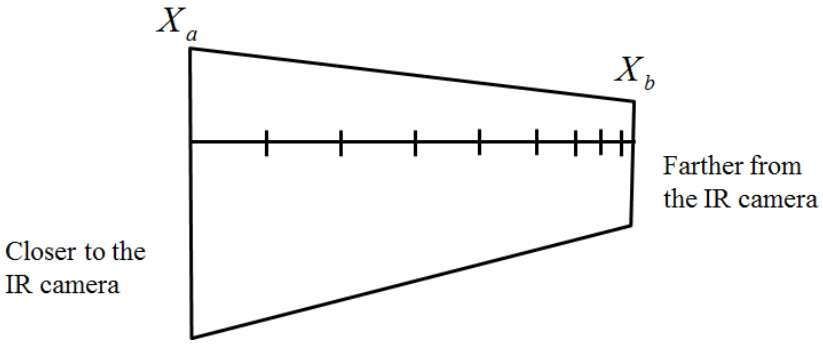


(c)

**Figure 4.5: Illustration of data fusion process**

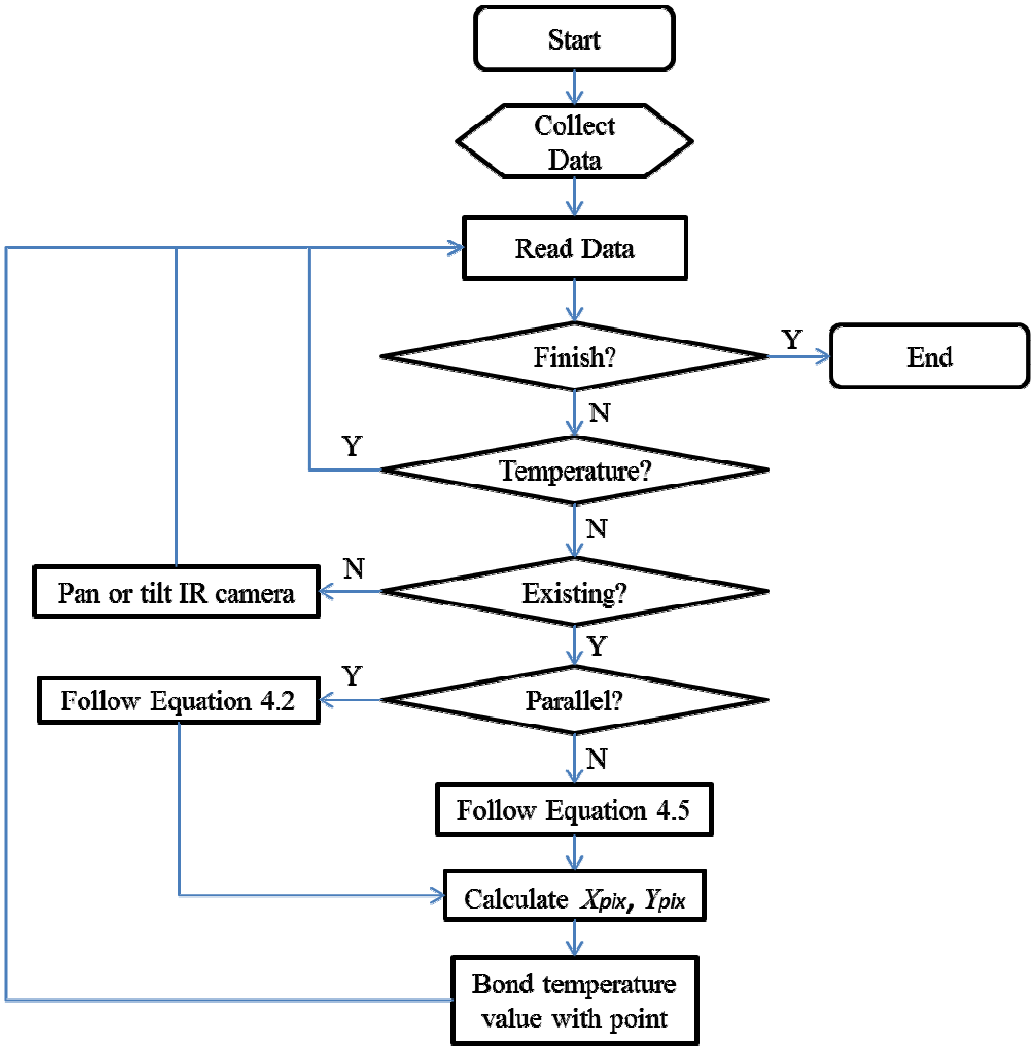


**Figure 4.6: Flowchart of temperature mapping process**

During the scan, each point collected by the system was considered as an object to find the corresponding temperature value according to the abovementioned equations. Figure 4.6 shows a flow chart of the proposed temperature fusion process with point clouds. The temperature fusion process continues until all the points have temperature values assigned. If a point does not contain temperature value, the program computes the angle $\alpha$ to determine if the object is parallel to the reference plane when the data are

collected. If it is parallel, Equation 4.2 is used to calculate $X_{pix}$ and $Y_{pix}$; otherwise Equation 4.5 will be used. Then the temperature value corresponding to $X_{pix}$ and $Y_{pix}$ in the temperature matrix is assigned to the point. After a loop, if any points remain without assigned temperature value, the IR camera is automatically panned or tilted to collect data.

### *4.3.3 Mapping Temperature Data to Window*

As mentioned earlier, it is difficult to map temperature data to a clear window because the beam passes through a transparent pane of glass. Similarly, the photogrammetry approach has the same problem with transparent windows since a digital camera cannot detect a clear window either. In the proposed method, the empty areas in point clouds that are unmatched with thermal data are recognized as panes of glass, and virtual points are created on the surfaces of the glass on which thermal data can be mapped.

In the created 3D thermal point cloud, each point's vertical coordinate is compared with its last vertical neighboring point. If the absolute value of the difference between them is greater than 20 units, the point itself and its neighboring point are respectively marked as lower and upper window boundary points. Then virtual windows can be created according to these window boundary points. Clear windows can be recognized in this way as shown in Figure 4.7.

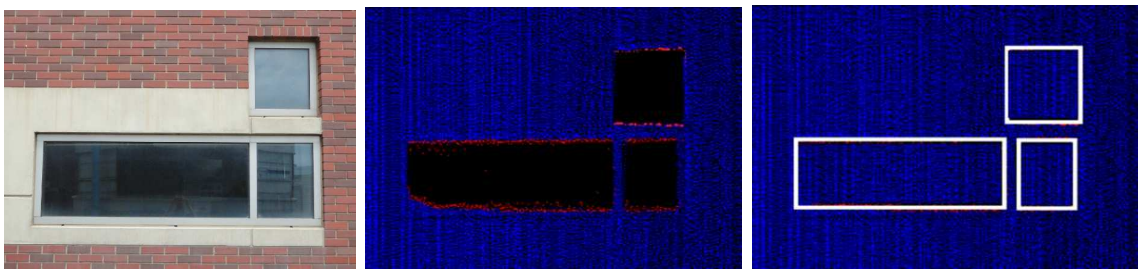

**(a)** **(b)** **(c)**

**Figure 4.7: (a) Digital image of clear windows; (b) Edge detection of the clear windows from a point cloud; (c) Creation of virtual points on clear windows**

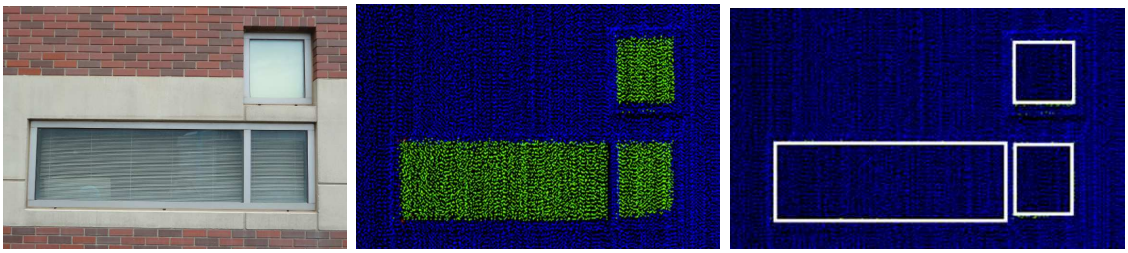

**(a)** **(b)** **(c)**

**Figure 4.8: (a) Digital image of blinded windows; (b) Blinds surface as recognized from the point cloud; (c) Creation of blinded window areas**

When collecting data from blinded windows, the laser beam went through the transparent glass and was reflected from the blinds. Two different surfaces were created, one from exterior walls and the other from the blinds, and the difference between these two surfaces could be used to recognize the blinded window glass. Based on the empirical value obtained through multiple experiments, the surfaces are recognized as two different surfaces if the absolute value of the difference between two surfaces is greater than 5 units and smaller than 10 units, as shown in Figure 4.8. Walls and blinds

are recognized as two different surfaces and rendered by two different colors, allowing the blinds area to be recognized as blinded window glass.

In the proposed method, all the threshold values were determined based on empirical analyses. To use the threshold effectively for a smaller window, higher resolution of point clouds is necessary to accurately recognize the window frame boundaries. For the complicated type of window, additional algorithms are needed to be added to make the proposed method more robust.

Once window areas were recognized, virtual points could be created inside the window frame according to certain vertical and horizontal interval values. Then, all the created virtual points could be fused with the corresponding temperature data as described in the section *Temperature Data Fusion.*

### 4.4 Full Field Tests and Discussion

Preliminary field test subjects were a "living laboratory" residential house called the Zero Net Energy Testing Home (ZNETH), shown in Figure 4.9 (a), and a part of the Peter Kiewit Institute (PKI) building at the University of Nebraska, shown in Figure 4.10 (a). The test on the ZNETH house was conducted on a hot and sunny day. Multiple thermal and laser scans were made to cover the whole building envelope. The captured thermal data were automatically registered and stored to point clouds on the building surface. After all the point clouds with thermal data were registered, they were rendered by different colors according to the normalized temperature value that was calculated by projecting lowest-highest temperature to 0-1. Here, 0 stands for blue, 1 stands for red. A simple mouse click on any point in the point clouds from the GUI shows x-y-z

coordinates and temperature value. For example, a hot point selected in Figure 4.9 (c) shows 39.566°C. The window detection algorithm was applied to the ZNETH thermal model as shown in Figure 4.9 (c), which can be compared to the 3D thermal point cloud without windows detection in Figure 4.9 (b). Precision and recall (Olson and Delon 2008) were estimated to evaluate the performance of the detection algorithm. As shown in Table 4.1, True Positive (TP) indicates the number of correctly recognized components, False Positive (FP) means the number of wrongly recognized components, and False Negative (FN) is the number of components that were not recognized. Six same size windows in the front wall of ZNETH were analyzed to compare the actual window size with the modeled window size. It can be seen from Table 4.2 that the average error difference is 6.30% for width and 10.85% for length.

(a)

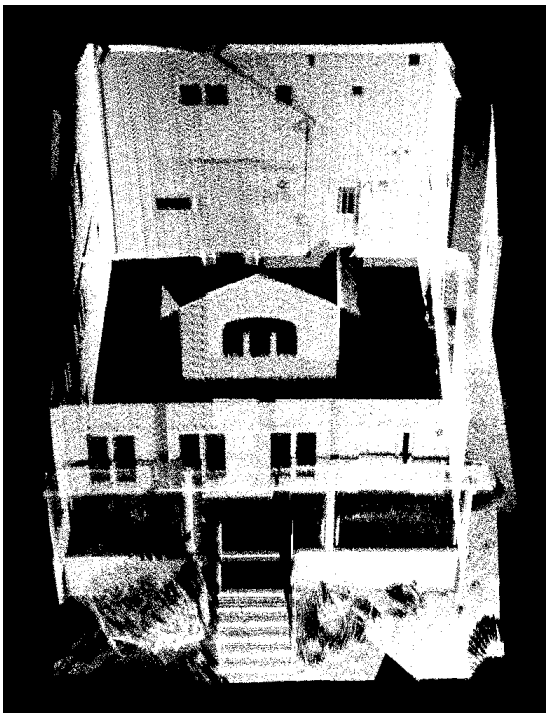

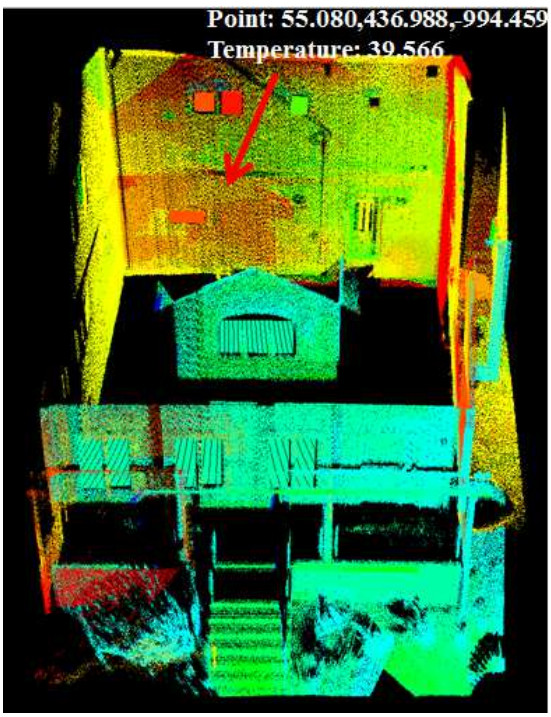


(b) (c)

**Figure 4.9: (a) Digital image of ZNETH; (b) 3D point cloud of ZNETH; (c) 3D thermal point cloud rendered by different colors based on normalized temperature values**

**Table 4.1: Precision and recall of windows recognition**

| Component | TP | FP | FN | Precision (%) TP/(TP+FP) | Recall (%) TP/(TP+FN) |
|---|---|---|---|---|---|
| Windows | 21 | 0 | 4 | 100 | 84 |

**Table 4.2: Error analysis of windows recognition**

| Component | Dimension | Actual Size (cm) | Recognized Size (cm) | Difference (%) |
|---|---|---|---|---|
| Window | Width | 50.80 | 47.60 | 6.30 |
| | Length | 139.70 | 124.54 | 10.85 |

Another set of tests was conducted with the PKI building to study the solar radiation effect. The tests were conducted during the day (2 pm) and at night (4 am). As shown in Figure 4.10, during the day, the same exterior building façade shows significant temperature differences because of solar radiation and shade. Points A and B in Figure 4.10 were randomly picked from each building façade. It can be seen from Table 4.3 that the shaded façade had a lower temperature. The daytime temperature difference between point A and B was about 7.5°C, but the nighttime difference was only about 1.8°C. Through the comparison, the effect of solar radiation was well observed, confirming that the building envelope's thermal data should be collected after the building cools off at night.

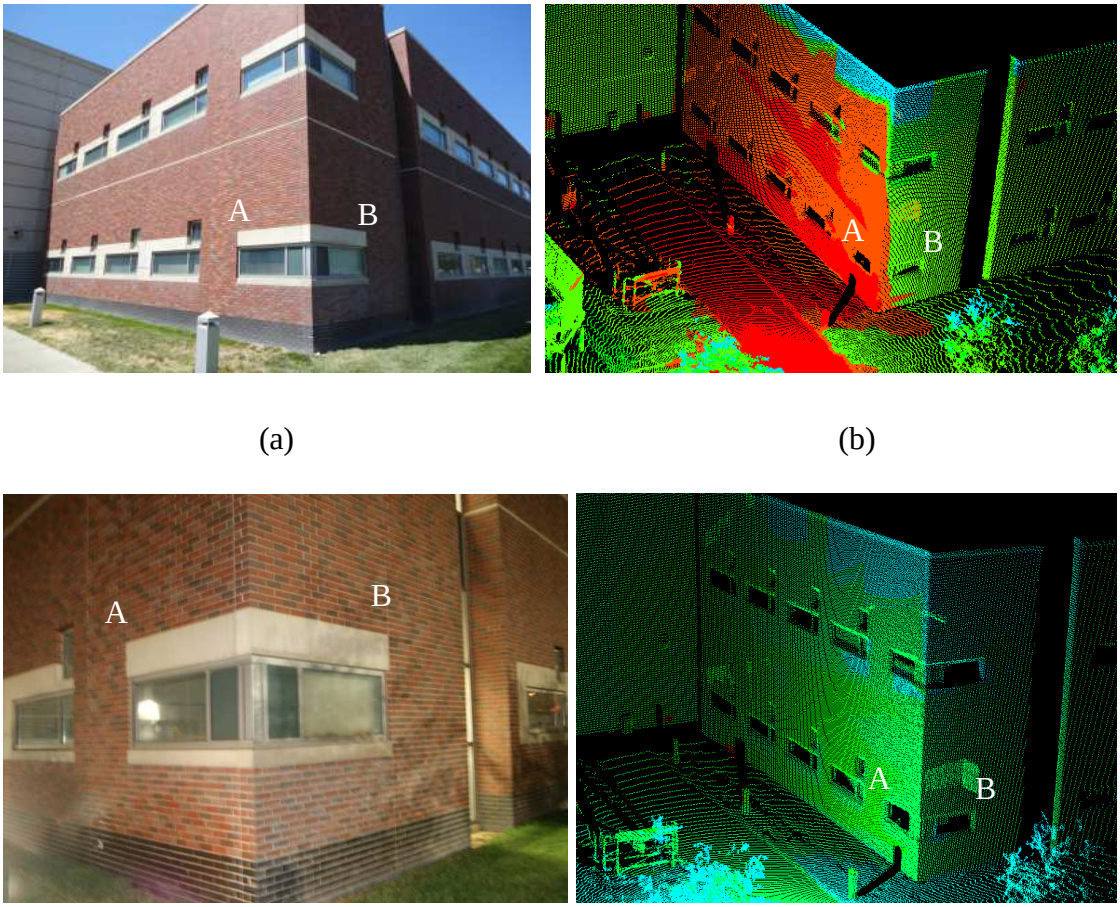


(a) (b)

(c) (d)

**Figure 4.10: (a) Daytime digital image of PKI building; (b) 3D thermal model created during the daytime; (c) Digital image of PKI building at night; (d) 3D thermal model created at night**

**Table 4.3: Temperature value of points A and B at daytime and nighttime**

| | Point A (°C) | Point B (°C) | A-B (°C) |
|---|---|---|---|
| Daytime | 39.167 | 31.622 | 7.545 |
| Nighttime | 24.431 | 22.661 | 1.770 |
| Daytime -Nighttime | 14.736 | 8.961 | NA |

A 3D thermal building model is ready to view as soon as the data are captured, which allows onsite modeling quality assurance. The proposed system is able to collect data at night to avoid the thermal effects of solar radiation and to accurately detect heat transferred through a building envelope. This is a strong advantage over the system that uses digital camera images. Also, the proposed system is designed to collect thermal data simultaneously while the laser scans a building, followed by immediate data fusion. It took about 20 minutes for each scan, including time to move and set up the system. After all the scans were finished, the only process remaining was to automatically register those sets of 3D thermal point clouds using the developed registration algorithm, which will be introduced in a future publication. Table 4.4 summarizes the differences among the proposed method and other state-of-the-art approaches.

**Table 4.4: Summarized differences between the proposed method and existing methods**

| | **EPAR** (Ham et al. 2012) | **Bi-Camera** (Alba et al. 2012) | **Irma3D** (Borrmann et al. 2012b, 2012c) | **Proposed Hybrid LIDAR** |
|---|---|---|---|---|
| **Data collection equipment** | Handheld IR camera with built-in digital camera (320x240) | IR cameras (320x240, 640x480) digital camera and 3D laser scanner | Fixed IR camera (160x120) mounted on a 3D laser scanner | 2 DOF robotic IR camera (320x240) integrated with a laser scanner |
| **Thermal data fusion process** | Automatic; IR image to digital image; 3D reconstruction using SFM | Manual; IR image and digital image to 3D point cloud; or 3D reconstruction with images using SFM | Automatic; IR image to 3D point cloud | Automatic; absolute temperature value to 3D point cloud (no image used) |
| **Data collection time** | Daytime | Daytime | Nighttime | Nighttime |
| **Thermal data reading** | Color | Color | Color | Color and text |
| **Other performances** | Lower equipment cost; low man power; good mobility; relatively lower model resolution and accuracy than laser scan-based approach; limited flexibility to upgrade IR or digital camera | Flexible to upgrade IR or digital camera; two sets of data group fusion (thermal images & digital images + point clouds & digital images) | Fast and real-time data fusion; robotic point clouds registration; limited vertical field of view due to the fixed camera position | Fast and real –time data fusion; high resolution of thermal model due to robotic scanning mechanism; thermal modeling for transparent windows (complete thermal modeling of building) |

## 4.5 Web-based Thermal Model Map

To improve connectivity between building energy performance information and the decision makers, a web-based geospatial program was utilized to display a 3D thermal map created from the proposed approach. To transfer the 3D thermal model to the geospatial program, a translation and rotation matrices were calculated to convert

point cloud data in the Cartesian coordinate system to the geospatial coordinate system (latitude, longitude, and attitude) (Im et al. 2012). To provide better visualization for the decision makers, ZNETH's BIM was imported into Google Earth Pro™.

The point cloud's Cartesian coordinates (x, y, z) need to be converted to latitude, longitude, and altitude (LLA) coordinates in order to be imported to Google Earth Pro™ through using transformation between LLA and earth-centered, earth-fixed (ECEF) coordinates as shown in Figure 4.11.

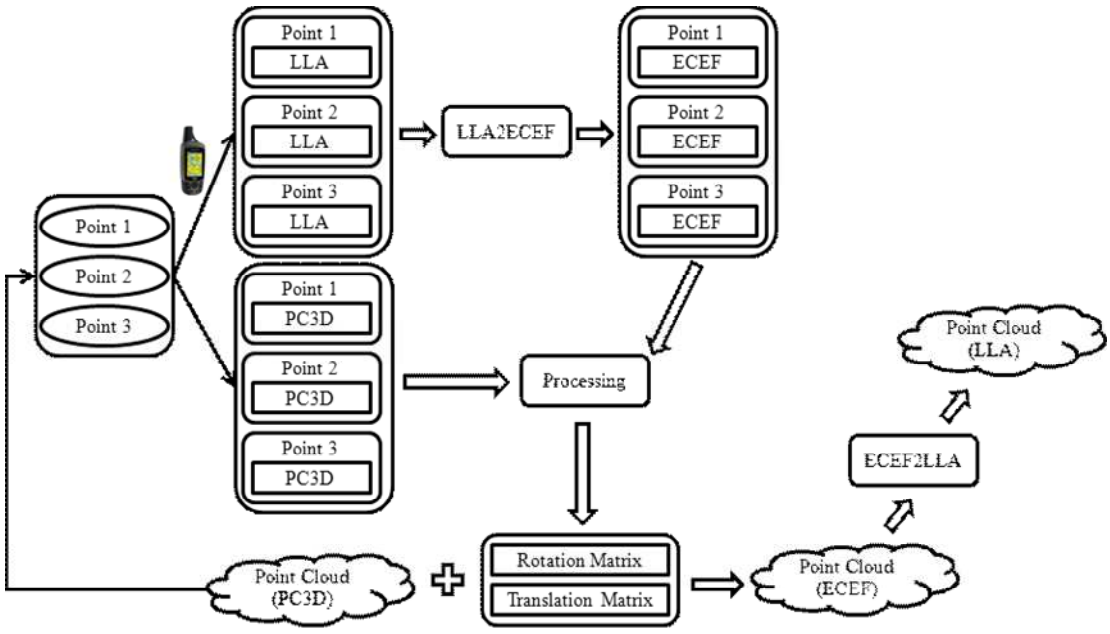


**Figure 4.11: The process of converting Cartesian coordinates to LLA coordinates**

Firstly, three LLA coordinates are measured by using a GPS receiver; meanwhile, three corresponding Cartesian coordinates of points with the same location in the point cloud are measured and stored. Then, these LLA coordinates are converted into ECEF coordinates through using the LLA2ECEF algorithm (Kleder 2005). As a result, three

corresponding coordinates in two different coordinate systems are obtained, which are Cartesian coordinates and ECEF coordinates.

All the points in the point cloud are then converted to ECEF coordinates through applying the rotation matrix and translation matrix. After being converted to ECEF coordinates, all the points are converted to LLA coordinates through using ECEF2LLA algorithm (Kleder 2006). At last, all the Cartesian coordinates in the point cloud are converted to LLA coordinates.

As shown in Figure 4.12, the 3D thermal point cloud and ZNETH's BIM were successfully imported into Google Earth Pro™, and all the thermal data were retained. The thermal data can be visualized by simply mouse clicking the corresponding point.


**Figure 4.12: 3D thermal BIM model of ZNETH in Google Earth Pro™**

## 4.6 Summary

This chapter introduces a rapid measurement system for a thermal 3D model of existing buildings. To rapidly and accurately measure the 3D geometries of a building envelope, a hybrid data collection system was developed. An IR camera was integrated into the 3D laser scanner to measure the temperature of the building surface. Multiple degrees of freedom (DOF) kinematics were solved to integrate the two units to obtain x-y-z coordinates and corresponding temperature data for each point. A GUI was developed to control the hardware units (laser scanner, PTU, and IR camera) for data collection and to edit and visualize 3D thermal point clouds. Window detection algorithms were introduced to create virtual thermal points on transparent window glasses and blinded windows. The technical feasibility of the developed hybrid system has been successfully demonstrated through two field experiments on a residential house and a commercial building.

# CHAPTER 5

# AUTOMATED GBXML-BASED BUILDING GEOMETRIC MODEL GENERATION

Although much work has been done on the processing of point cloud data for progress in construction and safety monitoring (Golparvar-Fard et al. 2009a), performance visualization (Golparvar-Fard et al. 2009b), and bridge management (Tang and Akinci 2012; Anil et al. 2013), not much work has been done to facilitate simulation of building performance. Further, as regards practicability, the current point clouds processing technologies are still in the very early stages.

The primary objective of this chapter was to provide a preliminary solution that automatically and rapidly extracts building envelope components of existing buildings from the thermal point cloud data that can be further utilized for building energy simulation applications. The thermal point cloud data collected from the hybrid 3D laser scanner system was processed to recognize different building envelope components such as windows, doors, walls, and roof as individual objects for gbXML-based geometry model generation. In the ensuing sections, this study first reviews the framework of the proposed approach, and then introduced the detailed automated geometric model creation process. Finally, field test results were discussed to validate the proposed framework.

## 5.1 The Framework for Automated As-Is Semantic Building Geometric Model Creation

The proposed method comprises four main steps: first, the collected raw data was pre-processed by removing noise data and downsizing the data. On the completion of data pre-processing, the region growing plane segmentation algorithm was applied to divide the raw data into segments of point cloud which were located at the same plane. Then, a boundary detection algorithm was introduced to recognize boundary points in each segment of point cloud. Further, all the detected boundary points were categorized into their own building component category and building geometry was successfully extracted. Figure 5.1 shows the flowchart for the proposed method. The four steps are explained in detail in the ensuing sub-sections.

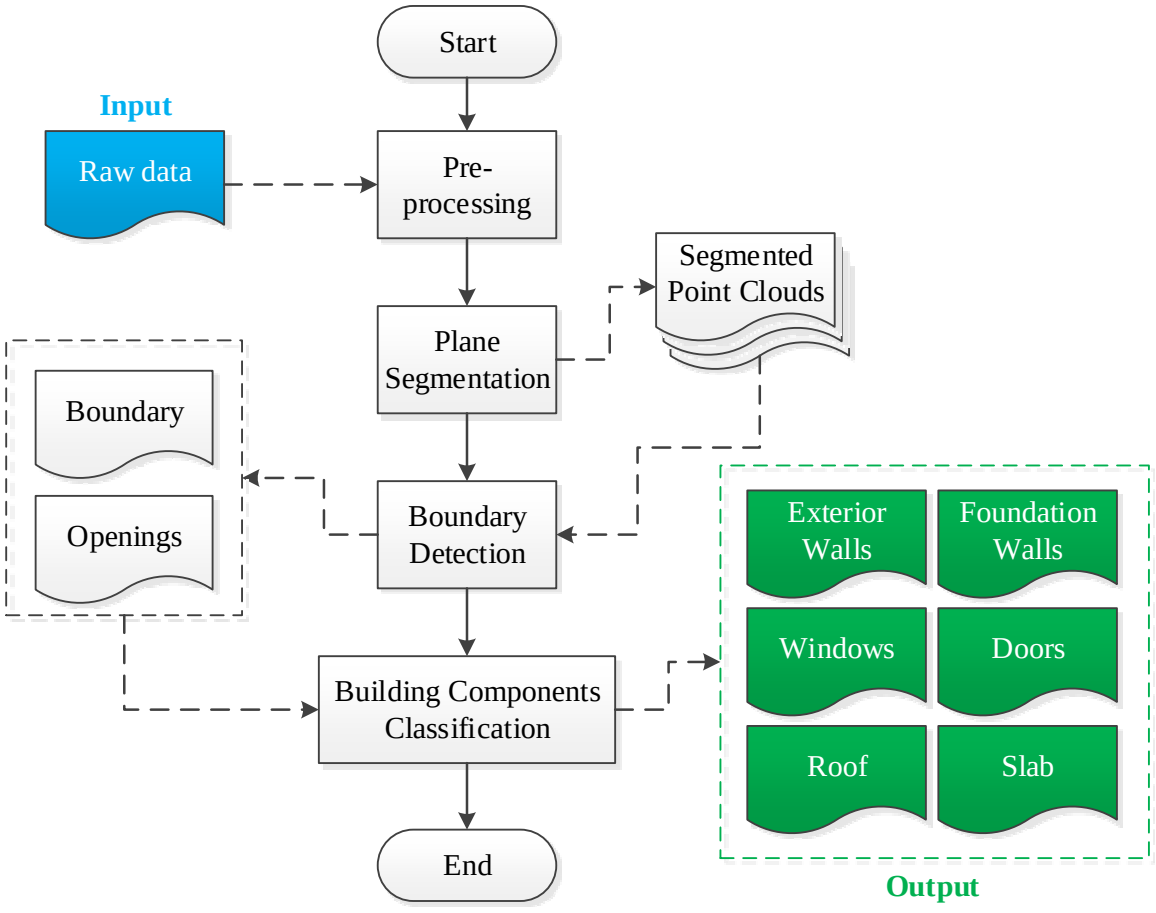


**Figure 5.1: Flowchart for the proposed method**

### 5.2: Data Pre-processing

The point cloud data collected by a laser scanner from an outdoor environment usually contain noise, which can result in a failure or inaccurate result if not being reduced or eliminated. A tensor voting algorithm (Kim et al. 2013) was employed in this paper to distinguish and remove the isolated points from the collected point cloud. The goal of data downsizing is to increase the data processing speed by reducing the amount of overly dense data being processed. The raw point cloud data are imported into a 3D space where the data structure is a 3D uniform voxel grid (Figure 5.2 (a)). Each voxel has its own specific boundary according to the size set up. After they are placed in their corresponding voxels, all the points present in the same voxel are removed and a centroid point for the point group is created (Moravec 1996) (Figure 5.2 (b), (c)). Thus, the bigger the voxel is, the more points are eliminated. The newly downsized data are then passed to the next step as input.

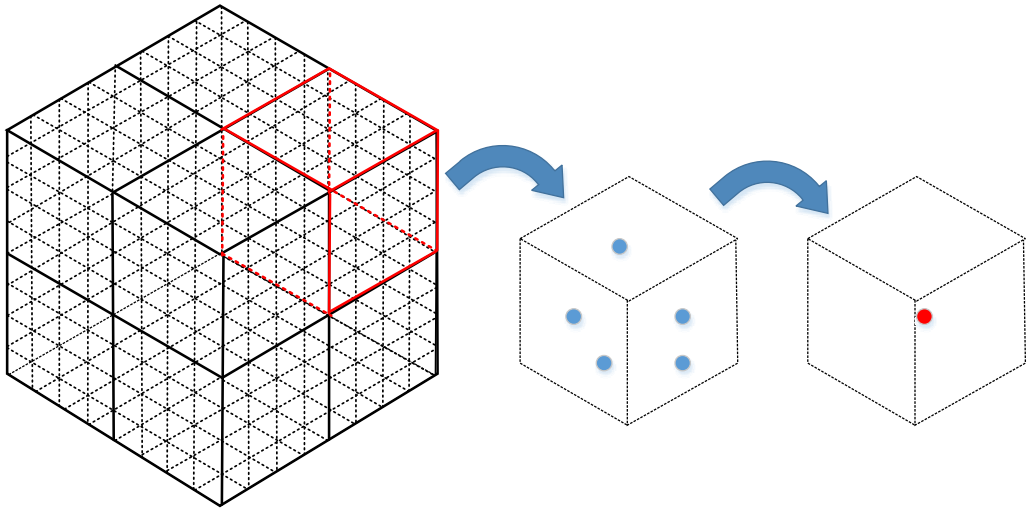


**Figure 5.2: (a) 3D uniform voxel grid structure; (b) a voxel and the points located in it; (c) one estimated point left after data downsizing (Illustration adapted from (Moravec 1996))**

### 5.3 Region Growing Plane Segmentation

In this research, existing residential buildings or small commercial buildings are mainly studied. Due to a difficulty of foundation form design and cost, most of the residential building envelope components have plane surfaces. Thus, a plane segmentation algorithm is then applied on pre-processed data to segment it into a set of disjoint point clouds which are located on the same plane. The region growing plane segmentation algorithm (Farid and Sammut 2012; Farid and Sammut 2013) was chosen in this research because of its desirable properties, such as conceptually simple and allowing applications in a wide range of settings. This algorithm can merge the points that are close enough to each other in terms of the smoothness constraint into one plane cluster. The algorithm sorts the points by their curvature value, and the region begins its growth from point $P$ with a minimum curvature value. This point $P$ is chosen and added to the set called seed points. For each seed point chosen, the algorithm finds its neighbor points $\{P_N\}$ and tests each neighbor point $N \in \{P_N\}$ for the angle between its normal and the normal of the current seed point. The current seed point is added to the current region if the angle is less than the threshold value $\theta_{th}$. Further, the curvature value of its neighbor point is compared with the value of the seed point. If the curvature value is less than the threshold value $C_{th}$, this neighbor point is added to the set of seed points and the current tested seed point is removed from the set. The algorithm repeats this process until the set of seed points is empty, signifying that the algorithm has grown the entire region and all points have been labeled. The output of this segmentation algorithm is a set of segmented point cloud clusters, where points in the same cluster are considered to be part of the same plane.

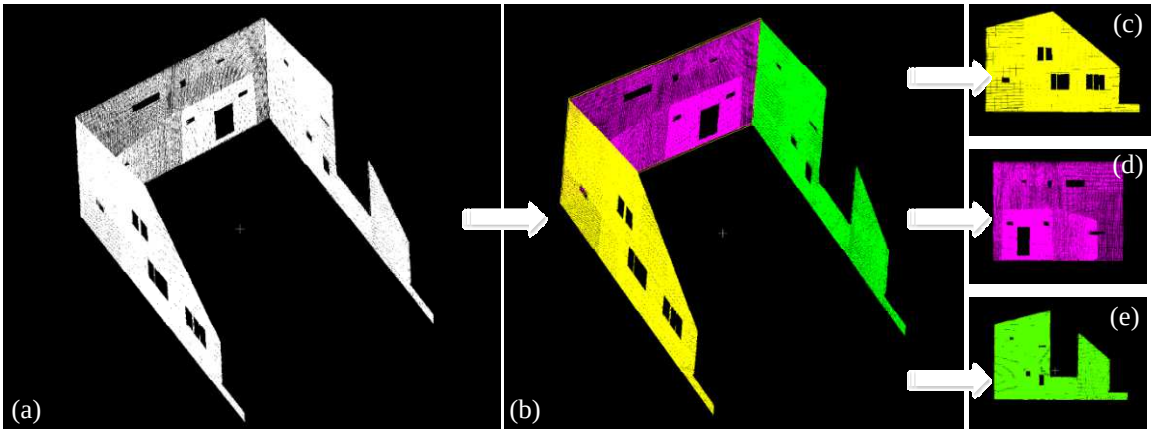


**Figure 5.3: Segmented point cloud clusters**

### 5.4 Edge and Boundary Point Extraction

Point cloud data cannot be collected from materials that have low reflectivity, such as black objects and glass, owing to the characteristics of the laser beam. Consequently, there is no point showing in the window glass area. The edge points of the window frames can be separated from the joined boundary points on the basis that the boundary points of the window frame surround an empty window glass area. In the third step, an edge and boundary detection algorithm (Rusu et al. 2007, Bae and Lichti 2004) is used to isolate edge and boundary points from the rest. The results of the region growing plane segmentation process are a set of segmented point cloud clusters, in which each point contains X, Y, Z coordinates together with its normal and curvature flatness. As illustrated in (Bae and Lichti 2004), the edges of the objects can be extracted based on the curvature information because they are characterized by high changes in curvature. However, the boundary points residing on the outer boarder of the point cloud cannot be found based on curvature data as there is no change for these points. Since all points in each cluster are on the same plane, the point cloud can be projected onto a 2D plane. In

2D plane, the boundary points can be easily identified because the maximal angle formed by the vectors towards the neighboring points is larger for boundary points than for points are on the inside of the object. For point cloud data of buildings, the edge points and boundary points are correspondingly referred to the edge of the openings and the boundaries of walls or roofs (see Figure 5.4). On the edge and boundary points of all clusters being recognized, all the component surfaces can be created by applying 2D concave hull algorithm (Zhou 2005).

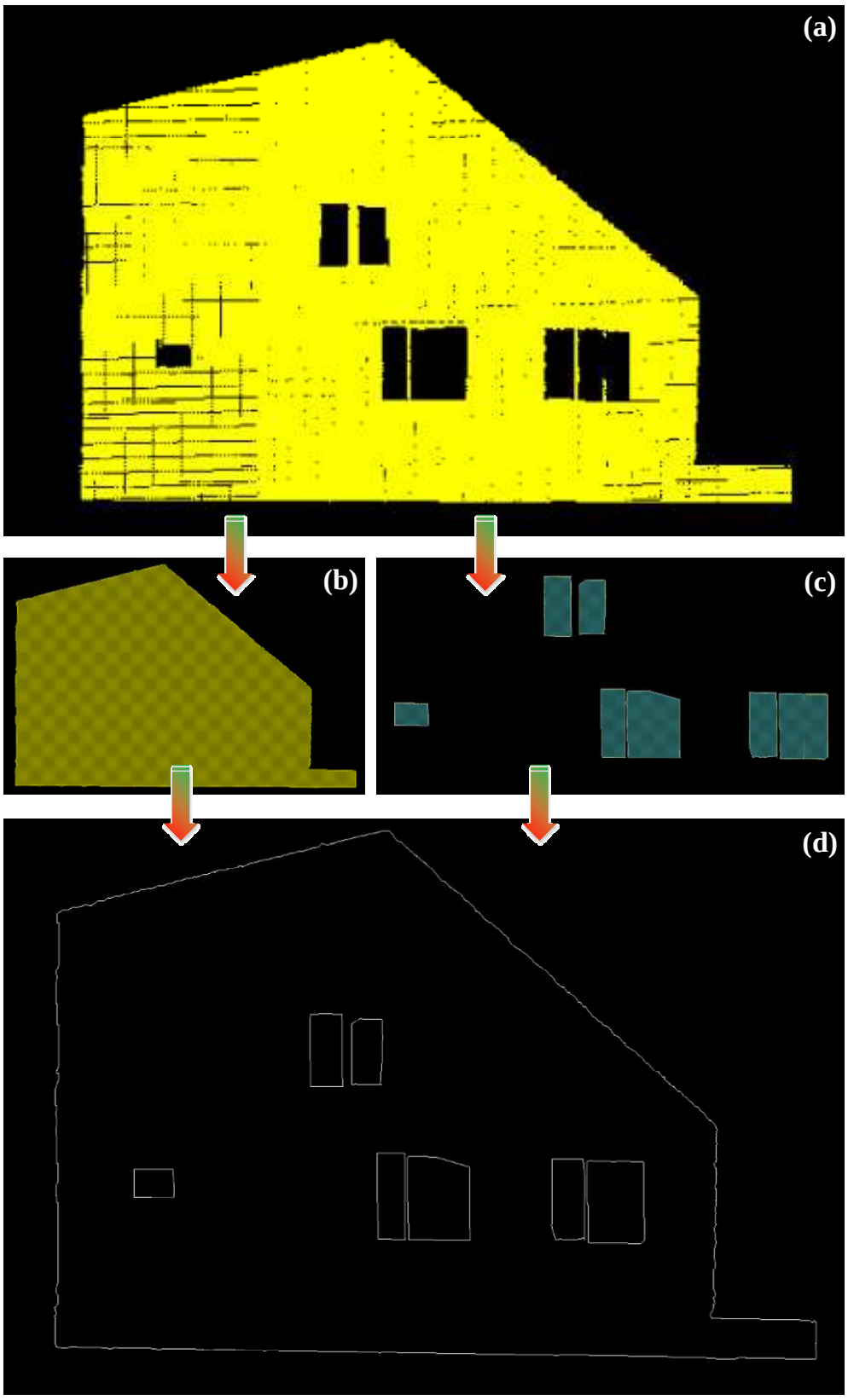


**Figure 5.4: Outer boundary and inner boundary recognition**

### 5.5 Rule-based Building Envelope Component Classification

In the final step of the proposed method, the building envelope components were automatically identified through the surfaces obtained from the previous sub-section. All surfaces recognized from the previous steps were processed through a rule-based classification system. The following rules were developed based on the understanding of the building features, and only the building components covered in the gbXML schema were considered in this research to be an object to recognize. First, all vertical surfaces were defined as wall components, then openings were separated from the recognized wall components. In this paper, it was assumed that all openings were closed when the data was collected. For each opening, if there was a same size of surface parallel and adjacent to it, then this paralleled surface can either be a door panel or window-blinds. Together with the location of the openings, the openings were labeled as a door if it was close to the bottom boundary of its wall surface, otherwise it was recognized as a window. The door components were further categorized into normal door and glass door according to the existence of the door panel. The window components were also categorized into clear window and blinded window based on the existence of a window-blinds. Figure 5.5 shows how an example of the recognized wall, window, door, and door panel surfaces. Then, the wall category was divided into two classes (exterior wall and foundation wall) by the rule that the foundation wall surface was below a door surface, and the exterior wall surface was not (Figure 5.6). The partial foundation wall surface could also be completed according to the user input. Because the roof was usually above the walls and adjacent to at least one exterior wall, it can be recognized once the exterior wall components are defined (Figure 5.7). Lastly, the unclassified surfaces were categorized

into raised floor and shade based on the rules that raised floor surface was horizontal and below a door surface, and shade surface was not adjacent to the space formed by wall surfaces. Table 5.1 shows the organized classification rules.

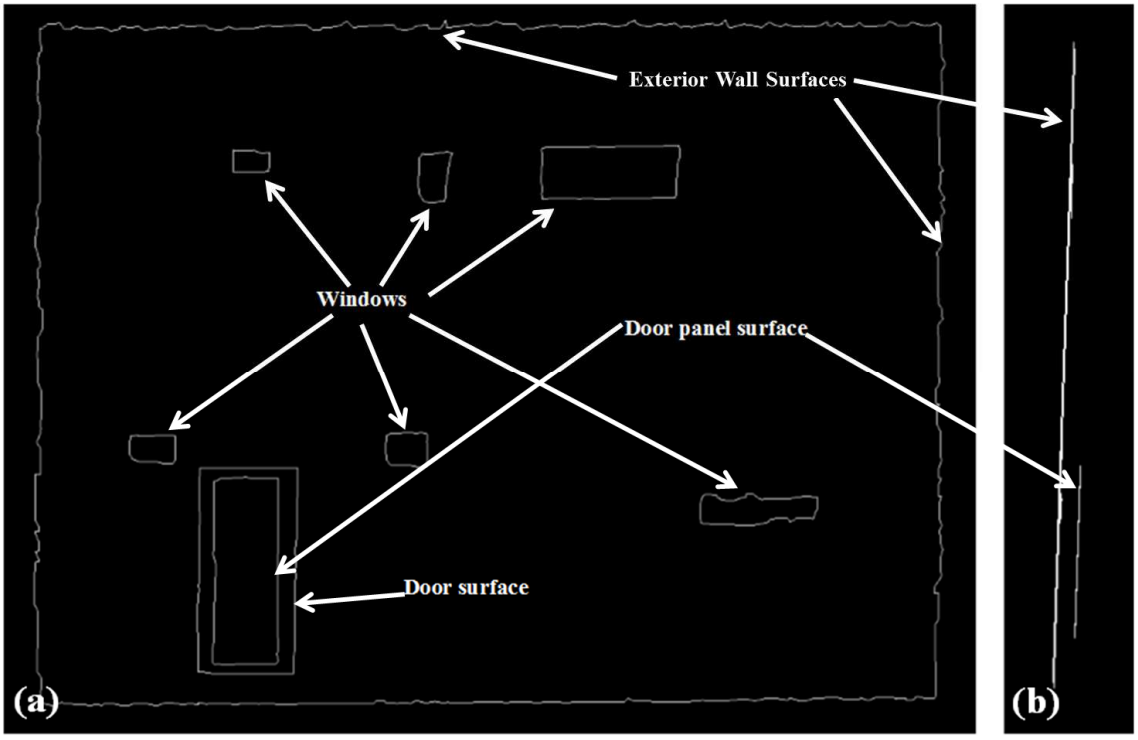


**Figure 5.5: Exterior wall surface and door panel surface (a) Front view. (b) Side view**

**Table 5.1 Proposed classification rules**

| Component | | Classification Rules |
|---|---|---|
| Wall | Exterior Wall | Vertical surfaces |
| | Foundation Wall | Vertical surfaces, below a door surface |
| Door | Panel Door | Bottom of the opening close to the boundary of the wall, panel surface behind the opening |
| | Glass Door | Bottom of the opening close to the boundary of the wall, no panel recognized |
| Window | Blinded Window | Non-door opening, blind surface behind the opening |
| | Clear Window | Non-door opening, non-blinded window |
| Roof | | Above and adjacent to exterior wall, non-vertical |
| Raised Floor | | Horizontal, below door surface |
| Shade | | Surface not adjacent to any spaces |

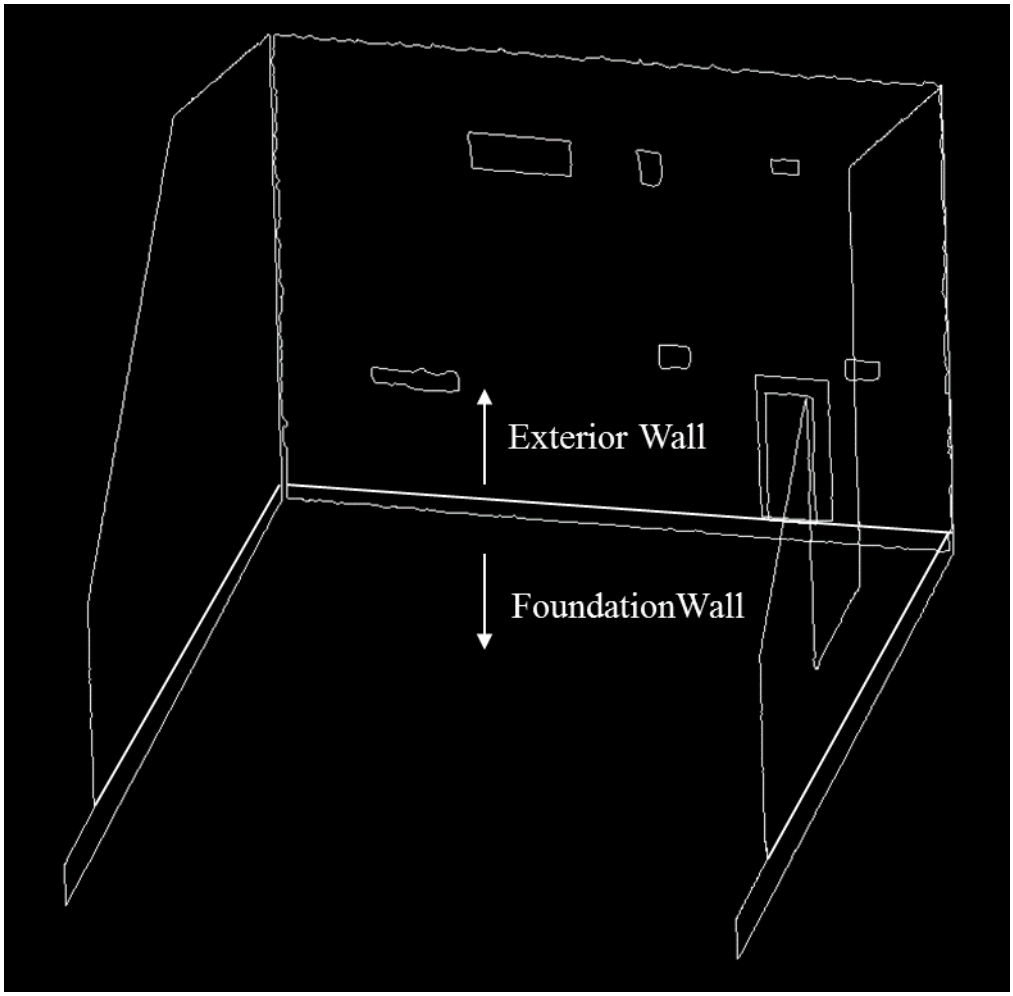


**Figure 5.6: Exterior wall and foundation wall**

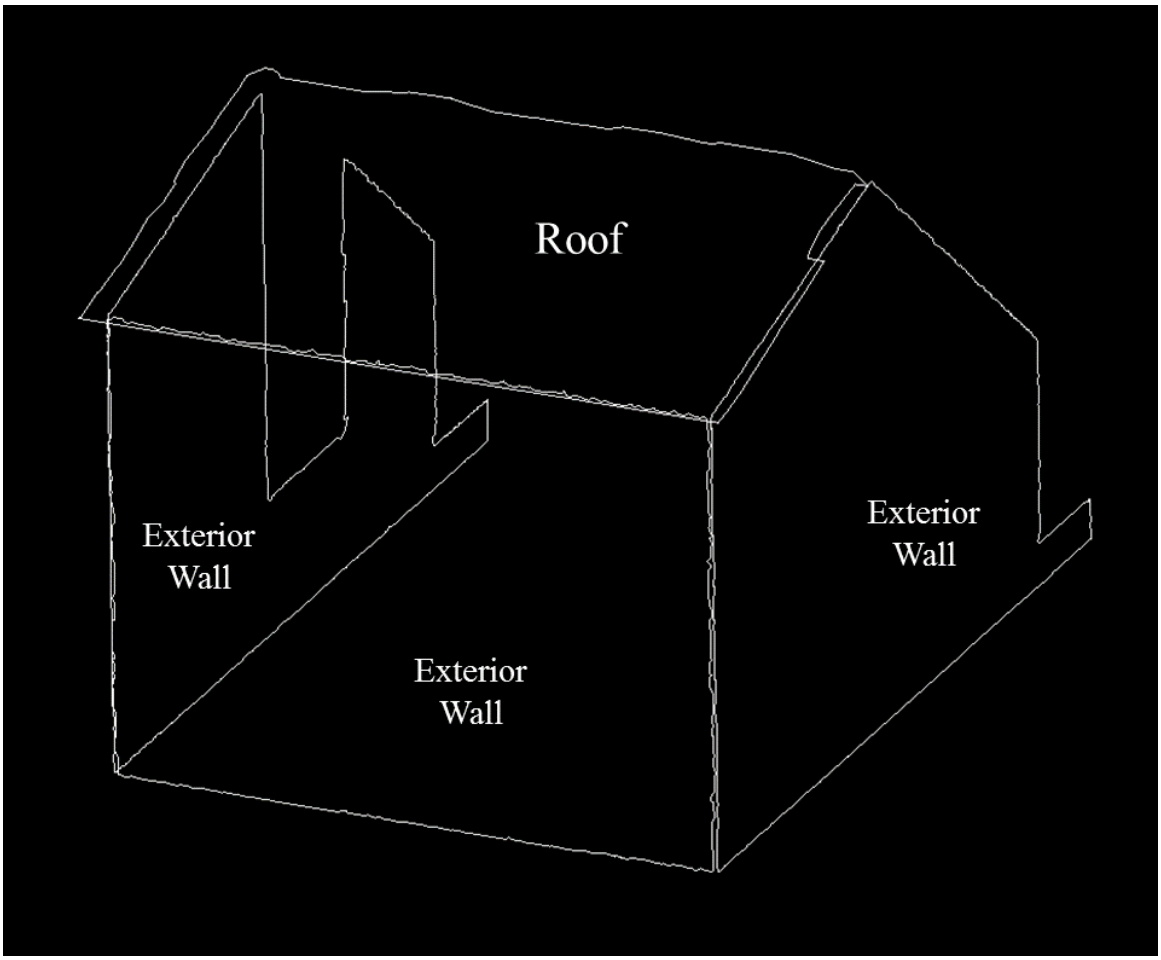


**Figure 5.7: Roof classification**

### 5.6 Geometry Size Fitting

Because the laser scanner has a limited scan resolution, and is unable to obtain thickness data of the envelope components. In Figure 5.8, it can be seen there are gaps between the recognized surfaces. Energy simulation requires a closed space as an input, therefore a geometry size fitting algorithm is needed to fill in those gaps. The proposed algorithm extended the surfaces of all walls, roofs, and raised floor, and replaced their surface edges with the intersection lines if existing (Figure 5.9).

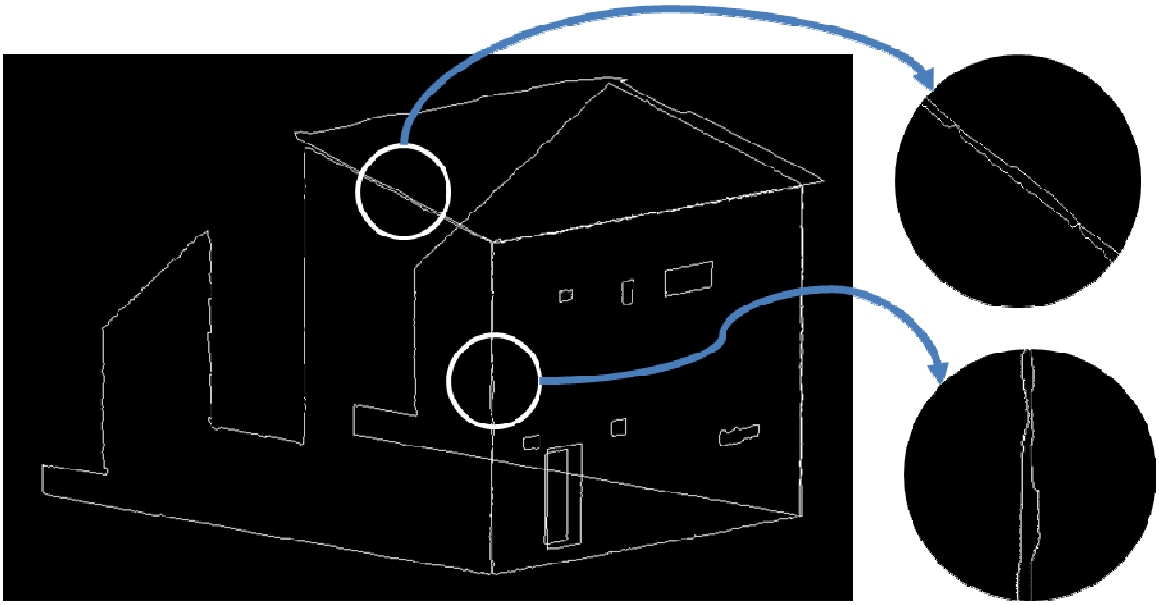

**Figure 5.8: Gaps between surfaces**

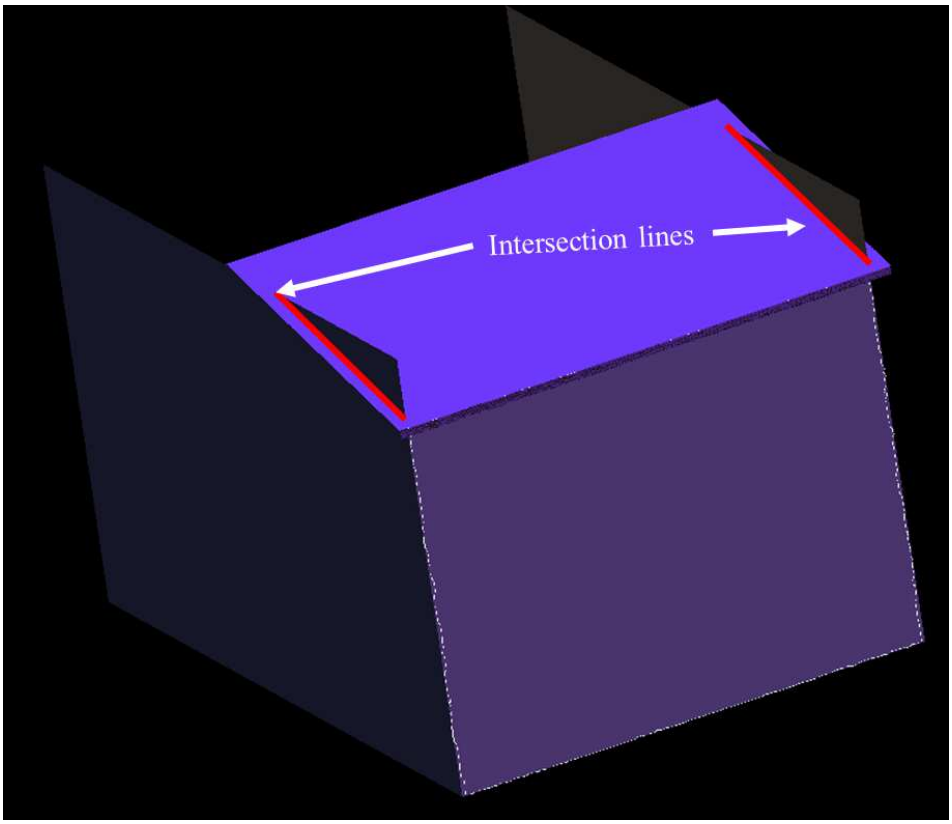


**Figure 5.9: Intersection lines extracted after surface extension**

## 5.7 Data Conversion

The output of the building component classification algorithm was a set of boundary points of the envelope components. For each individual component, all its boundary points were saved in a text file in which the first line of data was its surface ID, and followed by its surface type on the same line. Starting from the second line, there were three columns of data on each line, and they represented one point's x, y, and z coordinates. To be useful for energy simulation, the file has to be converted to another file format that can be imported. In this research, the gbXML open schema was chosen to help facilitate the transfer of the data to engineering analysis tools. Figure 5.10 is a structure chart of element "Surface" in gbXML schema (Version 5.0.1). This element was used to interpret the extracted components. Each surface requires a unique ID, surface type, and geometry. Surface type includes interior wall, exterior wall, roof, ceiling, and etc. In this paper, exterior wall and roof were assigned to corresponding surface. PlannarGeometry specifies the location of the surface, and lists all vertexes of the surface to define a loop. Attribute "Opening" is added if there is any opening in the surface. The extracted as-is data were first saved as text files, as shown in Figure 5.11, and then were converted into gbXML file according to the corresponding gbXML schema.

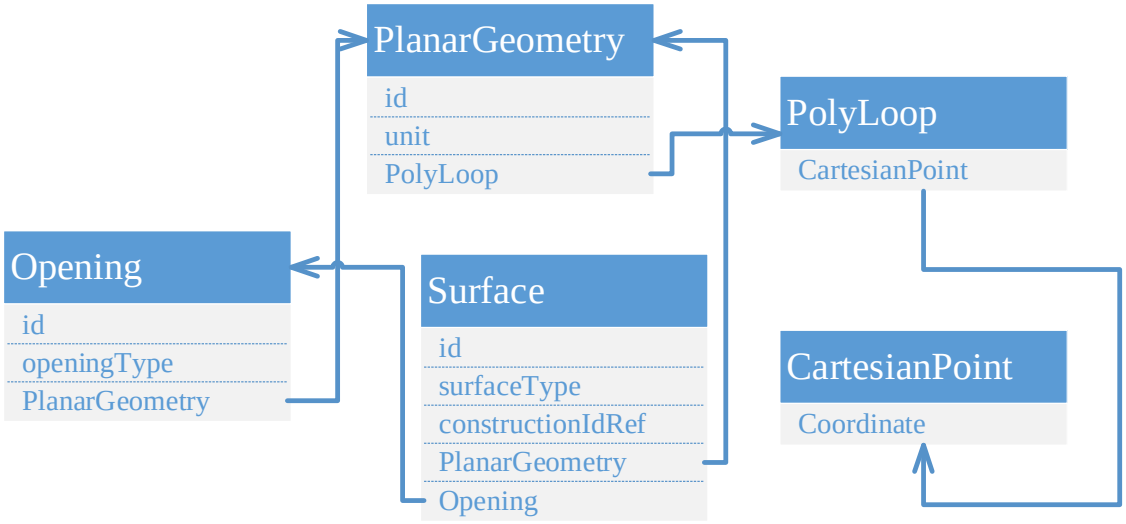


**Figure 5.10: The gbXML schema of the elements used in data exchange**

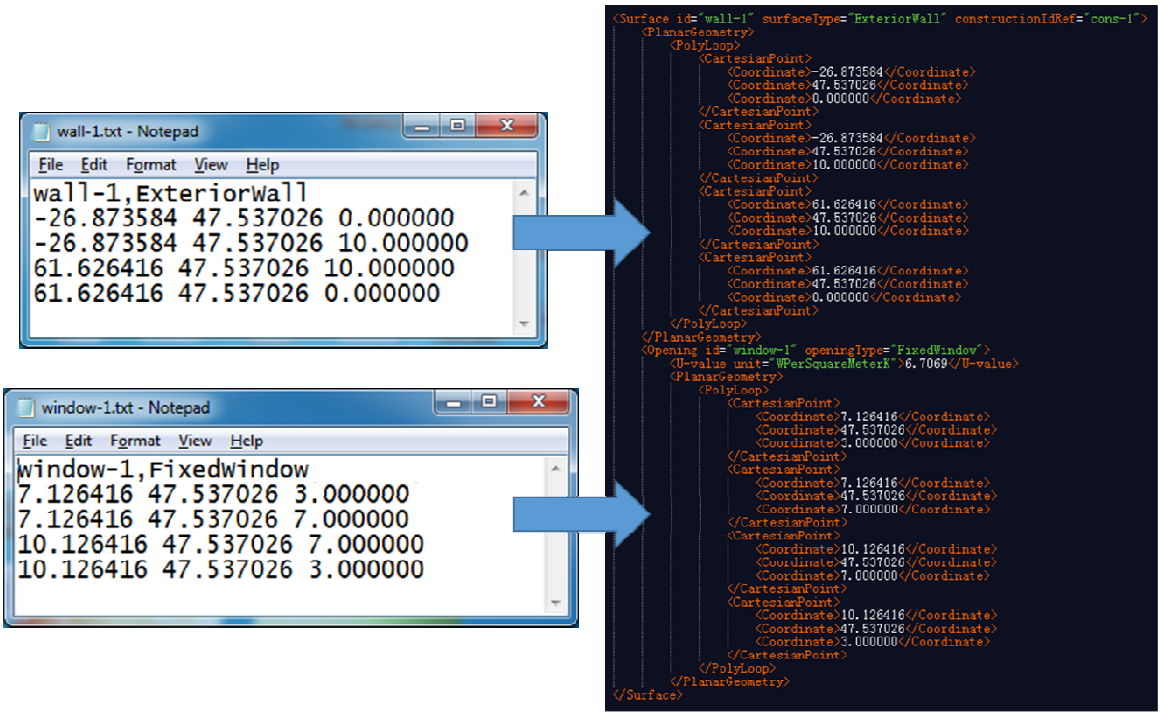


**Figure 5.11 Data exchange from text data (left) to gbXML data (right)**

### 5.8 Field Tests and Results

Validation of the proposed methodology was implemented on three small existing buildings, and two of which are residential houses, and one is a small bank building. In all case studies, the point clouds of the buildings were as completely as possible collected and used as raw input data. In the first cast study, the same residential house (ZNETH) that was tested in Chapter 4 was used as a test subject. The collected raw data (Figure 5.12(a)) containing 1,061,637 points were first processed by the data downsizing algorithm. In the algorithm, the leaf size of the vessel was set at 0.05m which is five times of the resolutions (0.01m) of the raw data. By utilizing data sizing algorithm, the data size was decreased to 541,003 points which is about half size of the raw data. The decreased data size can significantly reduce the processing time in the following processes. Then, the downsized point cloud data were segmented into a set of plane clusters (Figure 5.12(b)). For each segmented point cloud cluster, the inner and outer boundary points were extracted by a boundary and edge points detection algorithm.

The output of the boundary points detection algorithm was a set of outer and inner boundary surfaces. Then, the rule-based building envelope component classification algorithm followed to categorize each boundary surface into its corresponding category. Figure 5.12(c) shows the results of the proposed method. There were total 2 door components, 39 window components, 4 roof components, 1 underground wall component, 1 raised floor component, and 10 exterior wall components being recognized from the set of boundary surfaces. Precision, recall and accuracy (Olson and Delen 2008) were measured to evaluate the performance of the component classification (Table 5.2). In this case study, all recognized components excepted one window were correctly

categorized. The area dimensions of the recognized components were also compared with the manually measured area dimensions of the house, and the absolute difference was calculated for each recognized component. Table 5.3 shows the comparison results of the recognized geometry of each envelope component. The door category was the most accurately recognized in terms of the area size. The roof and exterior wall categories have a lower accuracy because the incompleteness of the raw data.

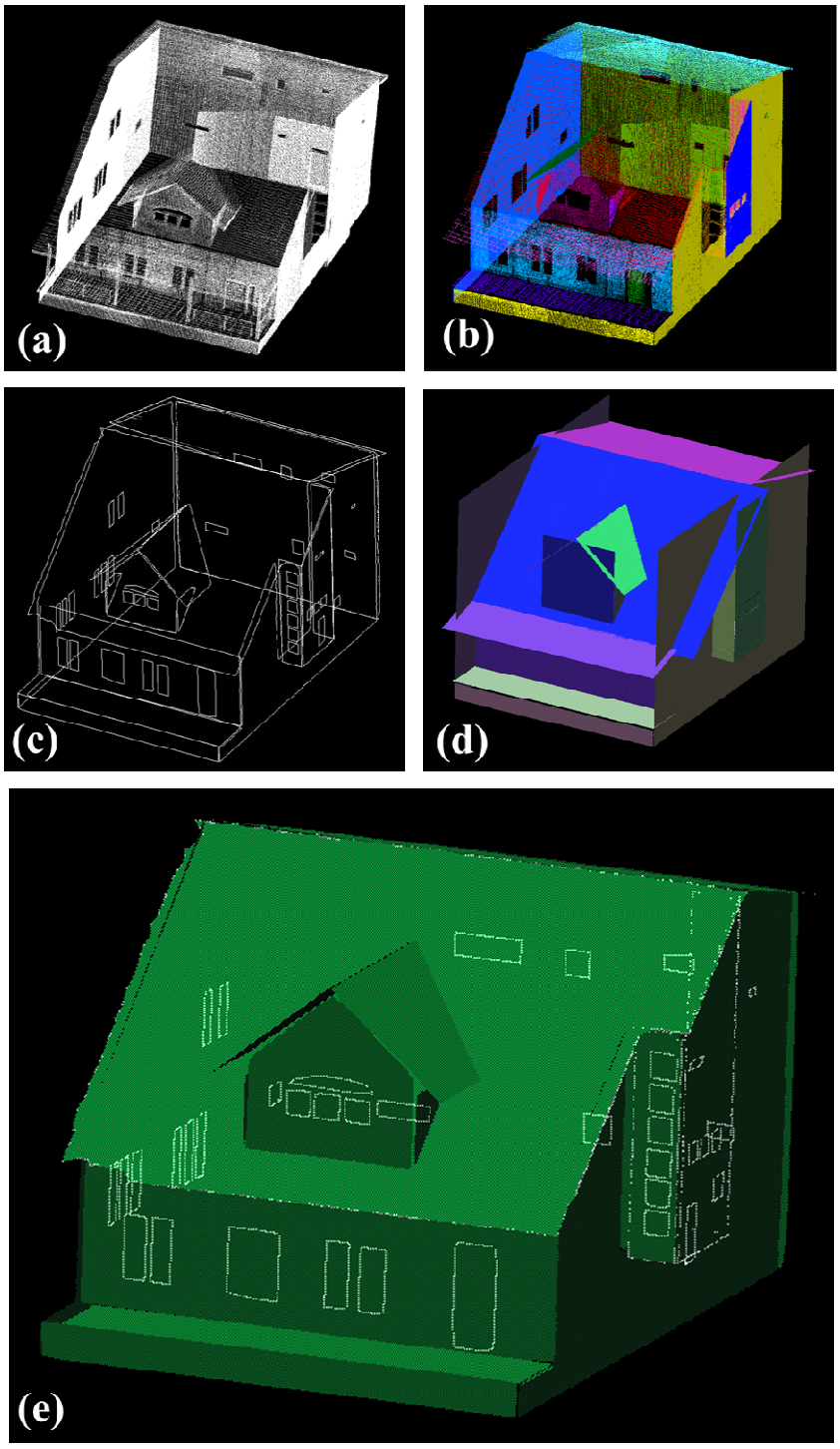


**Figure 5.12: Test results of case study 1 (ZNETH). (a) Raw data; (b) Segmented point cloud clusters; (c) Created semantic model; (d) Geometry size fitting**

**Table 5.2: Evaluation of the extracted envelope components for case study 1**

*Precision = TP / (TP+FP), Recall = TP / (TP+FN),*

*Accuracy = (TP+TN) / (TP+TN+FP+FN)*

| | TP | FP | FN | TN | Precision | Recall | Accuracy |
|---|---|---|---|---|---|---|---|
| **Exterior Wall** | 10 | 0 | 0 | 46 | 100.00% | 100.00% | 100.00% |
| **Window** | 39 | 0 | 1 | 17 | 100.00% | 97.50% | 98.25% |
| **Door** | 2 | 0 | 0 | 54 | 100.00% | 100.00% | 100.00% |
| **Foundation wall** | 1 | 0 | 0 | 55 | 100.00% | 100.00% | 100.00% |
| **Raised Floor** | 1 | 0 | 0 | 55 | 100.00% | 100.00% | 100.00% |
| **Roof** | 4 | 0 | 0 | 52 | 100.00% | 100.00% | 100.00% |

**Table 5.3 Comparison between the recognized and the manually measured envelope components for case study 1**

| | Measured Dimension ($m^2$) | Recognized Dimension ($m^2$) | Error ($m^2$) | Error (%) |
|---|---|---|---|---|
| **Exterior Wall** | 355.25 | 363.95 | 8.71 | 2.45 |
| **Door** | 3.90 | 4.27 | 0.37 | 9.49 |
| **Window** | 18.48 | 15.29 | 3.19 | 17.26 |
| **Roof** | 156.74 | 143.48 | 13.26 | 8.46 |
| **Raised Floor** | 19.74 | 16.41 | 3.33 | 16.87 |

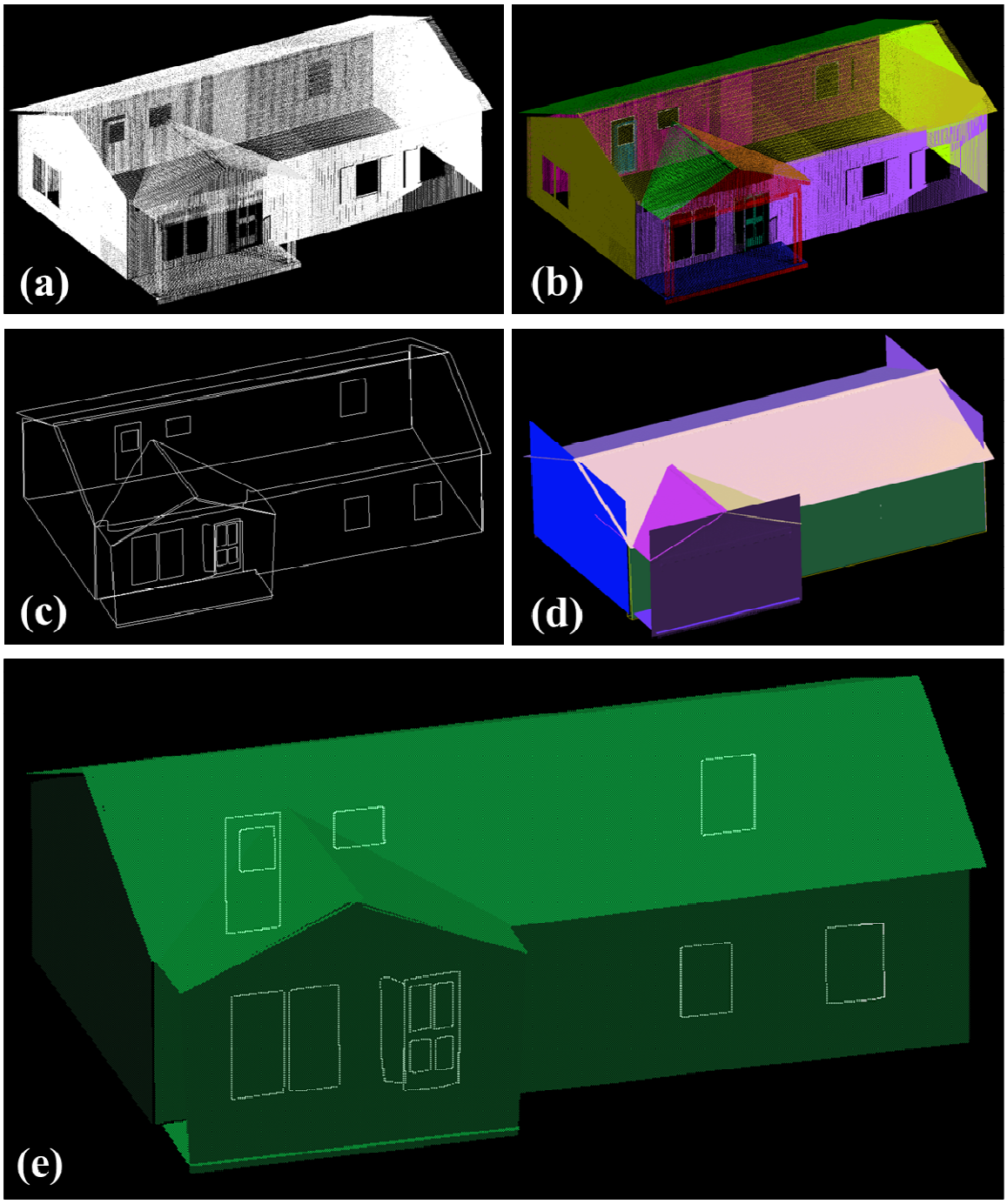


**Figure 5.13: Test results of case study 2 (ZNETH II). (a) Raw data; (b) Segmented point cloud clusters; (c) Created semantic model; (d) Geometry size fitting**

To further validate the robustness of the proposed methodology, two more case studies were conducted. As shown in Figure 5.13(a) and Figure 5.14(a), one is a one-story residential house, the other is a one-story bank building. Following the same process, the results of these two case studies were correspondingly visualized in Figure 5. 13 and Figure 5.14. The evaluation results of the component recognition were also shown in Table 5.5-5.7. In case study 2, one exterior wall and one door were falsely classified, and most components were recognized with around $1m^2$ error. There was 11.10 $m^2$ difference between the measured and the recognized roof components. This is also caused by the data incompleteness. In case study 3, the tested bank building has a more complicated roof containing 12 plane segments. Based on the evaluation results shown in Table 5.6, 3 out of 24 windows were not successfully recognized from the point cloud data. The dimension evaluation results in Table 5.7 shows that the recognized exterior wall and roof categories had greater absolute area difference compared with the manually measured one.

In Figure 5.15, all recognized component categories in three case studies were put together to analysis the relationship between the error and the measured area size of the component. It can be summarized from Figure 5.15 that the greater errors mostly came from the greater size of the component. Figure 5.16 shows the error range frequency, and total 50% of the recognized component categories had less than $2.5m^2$ error, and total about 71% had less than $10m^2$ error. Figure 5.16 shows the error range frequency, and total 50% of the recognized component categories had less than $2.5m^2$ error, and total about 71% had less than $10m^2$ error. Through a joint analysis with Tables 5.3, 5.5 and 5.7, it can be seen that the recognized component categories with greater than $10m^2$ error

are roof and exterior wall. This is because the point cloud data are usually difficult to be completely collected from these two components due to the building height or occlusion.

**Table 5.4: Evaluation of the extracted envelope components for case study 2**

*Precision = TP / (TP+FP), Recall = TP / (TP+FN),*

*Accuracy = (TP+TN) / (TP+TN+FP+FN)*

| | TP | FP | FN | TN | Precision | Recall | Accuracy |
|---|---|---|---|---|---|---|---|
| **Exterior Wall** | 4 | 1 | 0 | 20 | 80% | 100% | 96% |
| **Window** | 14 | 0 | 0 | 11 | 100% | 100% | 100% |
| **Door** | 2 | 1 | 0 | 22 | 67% | 100% | 96% |
| **Roof** | 4 | 0 | 0 | 21 | 100% | 100% | 100% |
| **Raised Floor** | 1 | 0 | 0 | 24 | 100% | 100% | 100% |

**Table 5.5 Comparison between the recognized and the manually measured envelope components for case study 2**

| | Measured Dimension ($m^2$) | Recognized Dimension ($m^2$) | Error ($m^2$) | Error (%) |
|---|---|---|---|---|
| **Exterior Wall** | 127.30 | 128.75 | 1.45 | 1.14 |
| **Door** | 2.97 | 3.89 | 0.92 | 3.10 |
| **Window** | 10.81 | 11.83 | 1.02 | 9.44 |
| **Roof** | 137.50 | 148.60 | 11.10 | 8.07 |
| **Raised Floor** | 10.41 | 10.19 | 0.21 | 2.02 |

**Table 5.6: Evaluation of the extracted envelope components for case study 3**

*Precision = TP / (TP+FP), Recall = TP / (TP+FN),*

*Accuracy = (TP+TN) / (TP+TN+FP+FN)*

| | TP | FP | FN | TN | Precision | Recall | Accuracy |
|---|---|---|---|---|---|---|---|
| **Exterior Wall** | 14 | 0 | 0 | 42 | 100% | 100% | 100% |
| **Window** | 27 | 0 | 3 | 26 | 100% | 90% | 95% |
| **Door** | 3 | 0 | 0 | 53 | 100% | 100% | 100% |
| **Roof** | 12 | 0 | 0 | 44 | 100% | 100% | 100% |

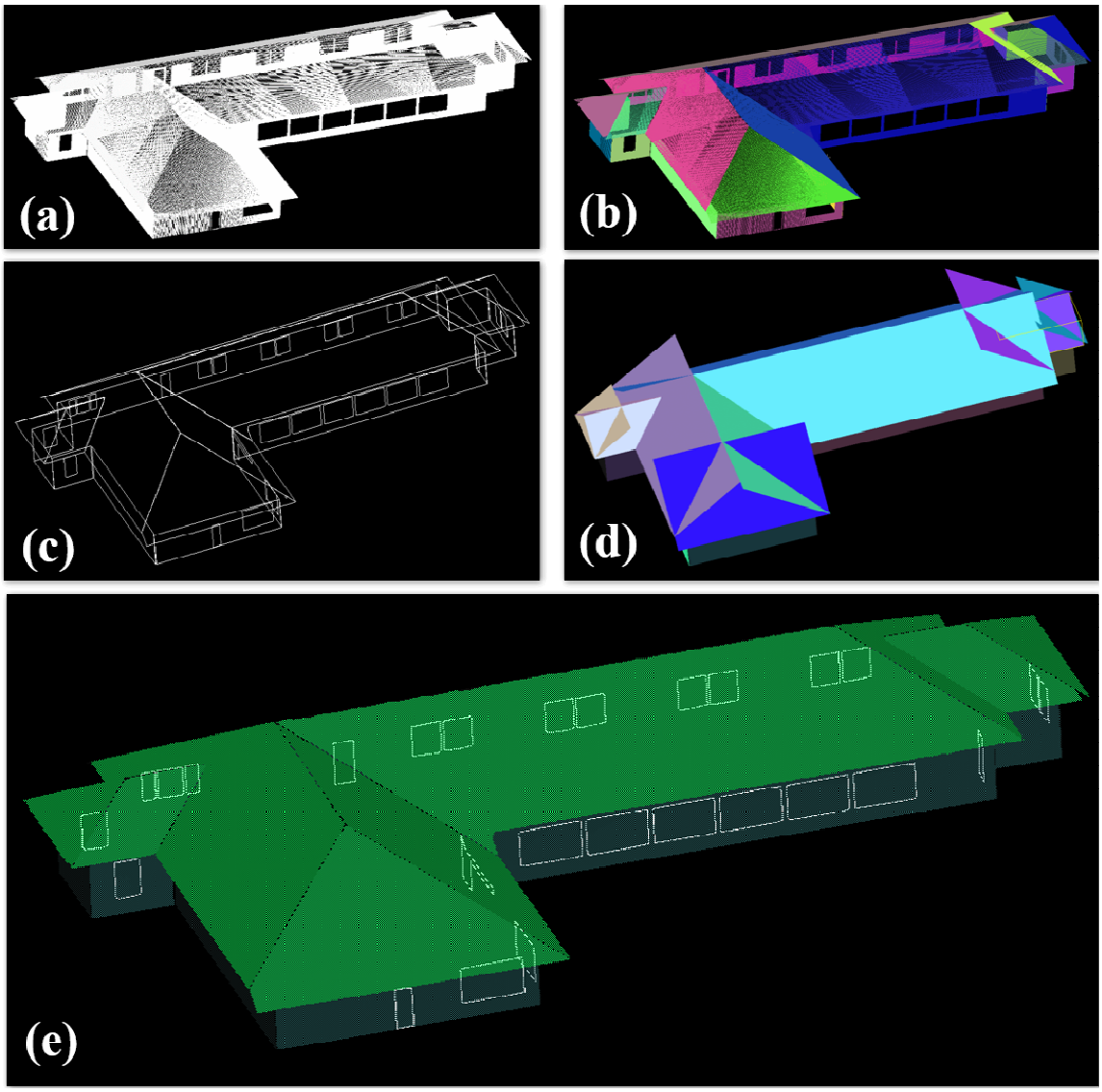


**Figure 5.14: Test results of case study 3 (Bank). (a) Raw data; (b) Segmented point cloud clusters; (c) Created semantic model; (d) Geometry size fitting**

**Table 5.7 Comparison between the recognized and the manually measured envelope components for case study 3**

| | Measured Dimension ($m^2$) | Recognized Dimension ($m^2$) | Error ($m^2$) | Error (%) |
|---|---|---|---|---|
| **Exterior Wall** | 347.70 | 324.74 | 22.97 | 6.61 |
| **Door** | 4.63 | 5.92 | 1.29 | 27.86 |
| **Window** | 76.01 | 77.53 | 1.52 | 2.00 |
| **Roof** | 1036.90 | 1054.00 | 17.11 | 1.65 |

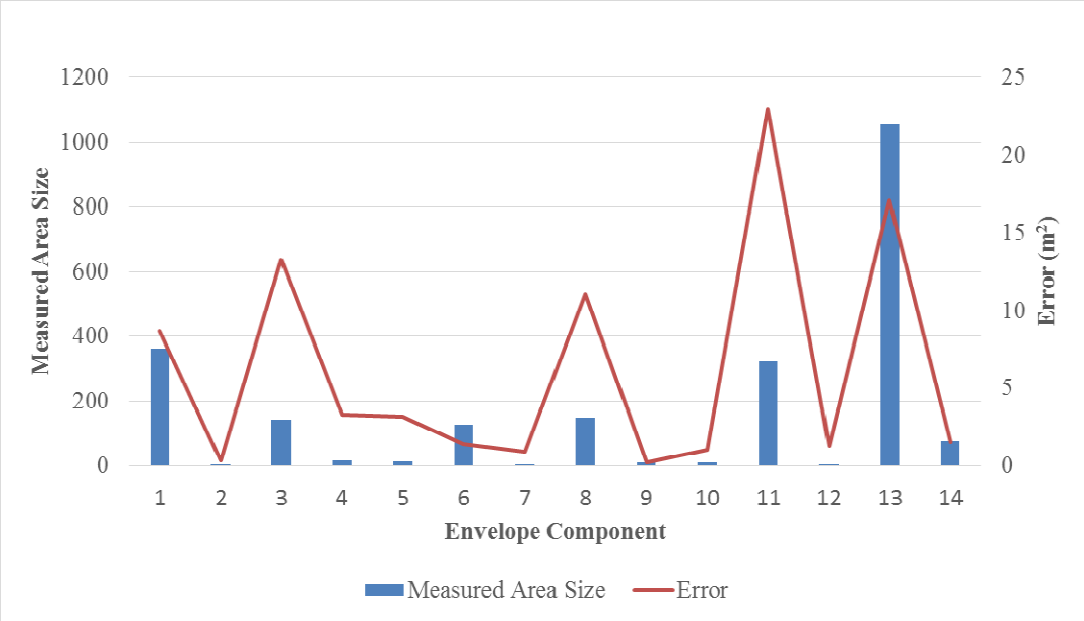


**Figure 5.15: Summary of the relationship between the error and the measured area size**

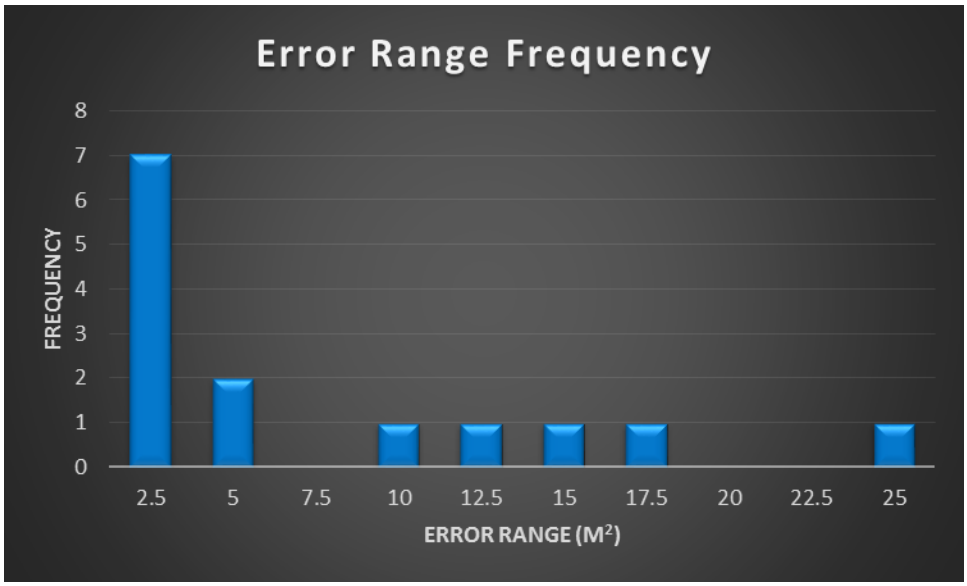


**Figure 5.16: Error range frequency**

## 5.9 Feasibility Validation

In previous sections, this study discussed about how to collect 3D thermal point cloud data, and how to automatically extract building envelope geometry from the point cloud data. The output from the previous sections was an auto-generated gbXML file. The intent of this section was to validate the feasibility of using the auto-generated gbXML file as an input in the energy simulation tools. Figure 5.14 shows the preliminary result that the auto-generated gbXML file of the case study 1 was successfully imported into a building energy simulation tool (Autodesk Ecotect Analysis 2011 was tested for validation in this study.).

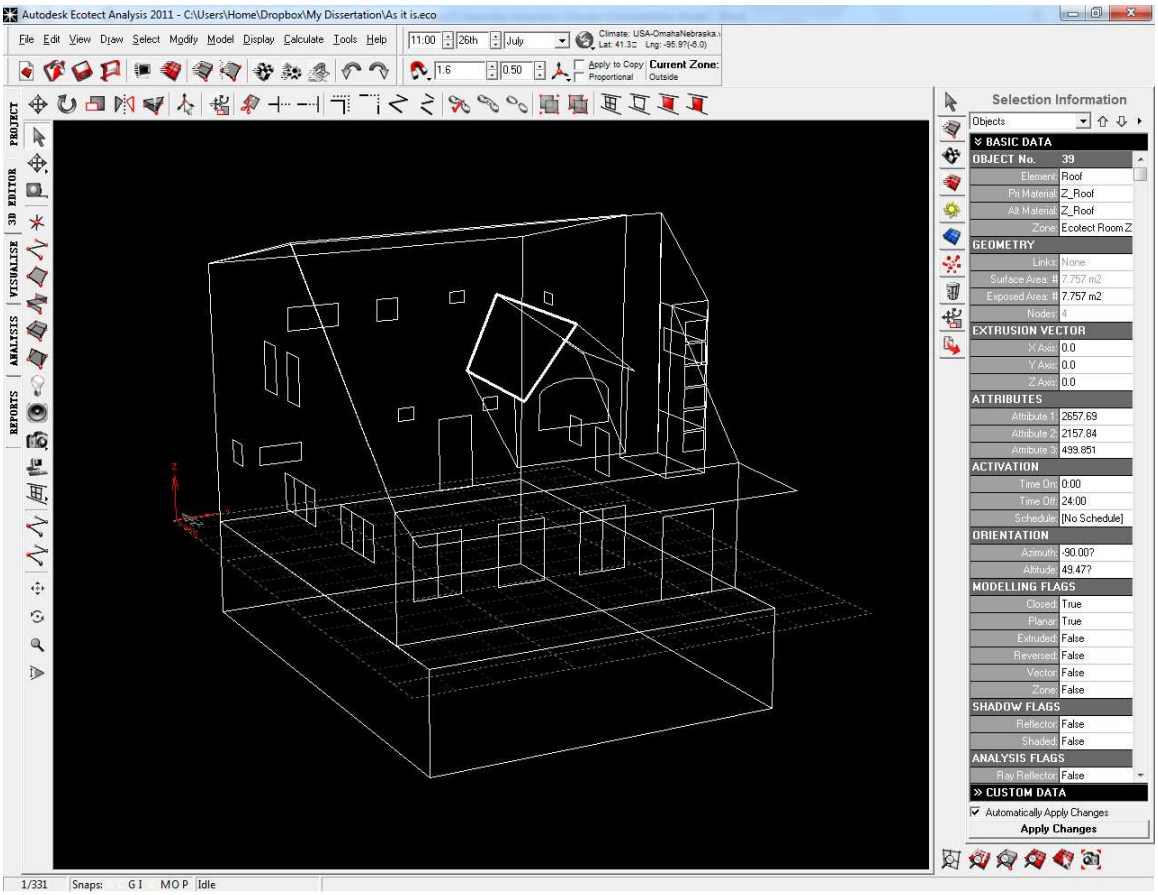


**Figure 5.17: Auto-generated gbXML file imported into Autodesk Ecotect**

## 5.10 Summary

In this chapter, this research proposed and demonstrated a method for automatic building geometry extraction from unorganized point clouds collected from a 3D laser scanner. In the proposed method, raw data were first eliminated to reduce the data size so as to increase the processing speed while maintaining accuracy. The downsized data were then processed through boundary detection algorithms, and building components finally recognized by processing the boundary points. The proposed method was tested and validated on three collected as-is building data. The test results show that the proposed method can successfully extract semantic information from the raw point cloud data, and convert the extracted data into a gbXML format that can be imported into the energy simulation tools. Precision, recall, accuracy of the component recognition algorithm, and dimension error of each component were all evaluated in this chapter.

# CHAPTER 6

# CONCLUSIONS

The intent of this chapter is to summarize and offer concluding remarks for this research. The chapter specifically addresses the research needs statement as well as the research questions presented in Chapter 1 of this research. Major findings of the research, identified limitations, and future research extension of this work are discussed in this concluding chapter.

## 6.1 Concluding Remarks

This research proposed a non-invasive methodology to automate the as-is 3D semantic geometric model creation process. Three research questions were presented in Chapter 1, and these research questions and a summarized discussion were presented in the following:

***Research Question 1:*** *How can the as-is point cloud and thermal data be non-invasively collected, fused and visualized?*

A hybrid data collection system was developed by integrating 2D laser scanners and IR camera. The laser scanner and the IR camera collected 3D point clod data and temperature data simultaneously. During the data fusion phase, the IR camera was calibrated and the kinematics of the system were solved to automatically map the collected temperature data. A 3D thermal point cloud can

be successfully created, and each point possesses its corresponding coordinates and temperature data. This study also discussed the effects of the sun radiation on the temperature data collection process, and concluded that it's best to collect data at dawn to avoid the sun radiation.

***Research Question 2:*** *How can the semantic data be automatically extracted from the collected raw data?*

A rule-based building envelope component recognition algorithm was proposed and created in this research. Using the 3D thermal point cloud as an input, this algorithm first downsampled the size of the input to reduce the total processing time. The downsampled point cloud data were then processed by a regional growing plane segmentation algorithm, and this algorithm segmented the downsampled point cloud data into a few clusters, in which all points have similar normal vector. Furthermore, an edge and boundary detection algorithm was introduced to extract boundary points in each cluster. Finally, a rule-based building component classification algorithm was developed to divide all plane segments into their corresponding categories, such as exterior walls, underground walls, windows, doors, roofs, shades, and raised floors. Field tests on selected residential houses were conducted to validate the feasibility of the proposed methodology and evaluate its performance as well. The test results showed that the precision, recall and accuracy of most of the extracted components can reach

95%, and the total about 71% of the recognized components had less than $10m^2$ error.

***Research Question 3:*** *How can the extracted semantic data be stored in terms of data interoperability?*

The extract components were first processed by a geometry size fitting algorithm to fill in the gaps between all the plane surfaces in order to create a closed space. All the extracted geometry data of the building components were originally saved as a text file, in which it included its component ID, adjacent component ID, and a set of boundary points. Based on the gbXML schema, this text data was automatically converted into a gbXML file. In the auto-generated gbXML file, the "surface" element stands for the plane segment. The auto-generated gbXML was also validated with the selected commercial building energy simulation software tools. The gbXML file was successfully imported, and all elements were correctly transported into the simulation tools.

## 6.2 Research Contributions

The contributions of this research include 1) a customized low-cost hybrid data collection system development to fuse various data into a thermal point cloud; 2) an automatic method of extracting building envelope components and its geometry data to generate gbXML-based building geometry model. The broader impacts of this research are that it could offer a new way to collect as is building data without impeding

occupants' daily life, and provide an easier way for laypeople to understand the energy performance of their buildings via 3D thermal point cloud visualization.

### 6.3 Limitations and Future Research

Despite of the demonstrated promising results, it is still inevitable that this research has a few limitations,

(1) The success of the proposed methodology totally depends on the completeness of the collected data. It's hard to recognize a building component that was occluded during the data collection or that has many noisy data

(2) The collected data usually contains other non-related objects, such as trees, other buildings, grounds, and cars. In this methodology, the unrelated data were manually filtered at the start.

(3) Compared to commercial buildings, the residential house has small and various shapes, which may challenge the robustness of this research. More case studies need to be conducted to increase the reliability of the proposed system.

In future work, this study will focus on improving the accuracy of processing incomplete data because it was identified that accuracy primarily relies on the integrity of the data. The data downsizing process can cause errors because it replaces the points in each voxel with an estimated point. Incomplete data is another factor that can reduce accuracy (e.g., the incomplete roof of the residential house and the parts blocked by trees and bushes). Therefore, how to complete the data and filter the unrelated data will also be an emerging topic. This research also plans to further enhance the robustness of the

proposed methods so that it can be implemented and used for several different types of object recognition and extraction activities for as-built modeling in the AEC/FM domain. Automatic indoor room zone creation will also be investigated in the future research, and it will be helpful for those buildings with more than one thermal zone. Lastly, the auto-generated gbXML files should be evaluated through comparing its simulation results with traditional method. In the long run, the future research outcomes are expected to stimulate decision makers to improve their buildings by providing reliable, visual information about their building's energy performance, thus benefiting the economy, society, and the environment.

# REFERENCES


Abeid, J., Allouche, E., Arditi, D., Hayman, M. (2003). "PHOTO-NET II: A computer-based monitoring system applied to project management." Automation in Construction, 12(5), 603-616.

Adan, A. and Huber, D. (2011). "3D reconstruction of interior wall surfaces under occlusion and clutter." 3D Imaging, Modeling, Processing, Visualization and Transmission (3DIMPVT), Hangzhou, China.

Akinci, B., Boukamp, F., Gordon, C., Huber, D., Lyons, C., and Park, K. (2006). "A formalism for utilization of sensor systems and integrated project models for active construction quality control." Automation in Construction, 15(2), 124-138.

Alba, M. I., Barazzetti, L., Scaioni, M., Rosina, E., and Previtali, M. (2011). "Mapping Infrared Data on Terrestrial Laser Scanning 3D Models of Buildings." Remote Sensing, 3(9), 1847-1870.

Alba, M., Fregonese, L., Prandi, F., Scaioni, M., and Valgoi, P. (2006). "Structural monitoring of a large dam by terrestrial laser scanning." Proc. ISPRS Commission V Symposium, ISPRS, Dresden, Germany.

Anderson, D., Herman, H., and Kelly, A. (2005). "Experimental characterization of commercial flash ladar devices." Proc. Int. Conf. Sensing and Technology. IEEE, Palmerston North, New Zealand

Anil, E.B., Tang, P., Akinci, B., and Huber, D. (2011). "Assessment of quality of as-is building information models generated from point clouds using deviation analysis." Proceedings of SPIE, San Jose, California, USA.

Anil, E.B., Tang, P., Akinci, B., and Huber, D. (2013). “Deviation analysis method for the assessment of the quality of the as-is Building Information Models generated from point cloud data.” Automation in Construction, 35, 507-516.

Autodesk. (2014). <http://www.autodesk.com/products/autodesk-autocad-plant-3d/overview>, (Jan. 27, 2014).

AVEVA Continual Progression. (2014). <http://www.aveva.com/en/Products_and_Services/Product_Finder.aspx#open:0F6798A9-0B3A-4E72-88C3-4BEC11228F5E>, (Jan. 27, 2014).

Azhar, S. and Brown, J. (2009). “BIM for sustainability analyses.” *International Journal of Construction Education and Research*, 5, 276-292.

Bae, K.-H. and Lichti, D. D. (2004). “Automated registration of unorganized point clouds from terrestrial laser scanners.” in International Archives of Photogrammetry and Remote Sensing (IAPRS), 222–227.

Balaras, C., and Argiriou, A., (2001). “Infrared Thermography for Building Diagnostics.” Energy and Buildings, 34(2), 171-183.

Bhatla, A., Choe, S., Fierro, O., and Leite, F. (2012). “Evaluation of Accuracy of as-built 3D Modeling from Photos taken by Handheld Digital Cameras.” Automation in Construction, 28, 116-127.

Bohn, J. and Teizer, J. (2010). “Benefits and barriers of construction project monitoring using high-resolution automated cameras.” Journal of Construction Engineering and Management, 136(6), 632–640.

Borrmann, D., Afzal, H., Elseberg, J., and Nüchter, A. (2012a). “Mutual Calibration for 3D Thermal Mapping.” Proceedings of the 10th International IFAC Symposium on Robot Control (SYROCO '12), Dubrovnik, Croatia, September 2012.

Borrmann, D., Elseberg, J., and Nüchter, A. (2012b). “Thermal 3D Mapping of Building Facades.” Proceedings of the 8th Conference on Intelligent Autonomous Systems (IAS '12), Jeju Island, Korea, June 2012.

Borrmann, D., Nüchter, A., Đakulovic, M., Maurovic, I., Petrovic, I., Osmankovic, D., and Velagic, J. (2012c). “The Project ThermalMapper – Thermal 3D Mapping of Indoor Environments for Saving Energy.” Proceedings of the 10th International IFAC Symposium on Robot Control (SYROCO '12), Dubrovnik, Croatia, September 2012.

Bosche, F. (2010). “Automated recognition of 3D CAD model objects in laser scans and calculation of as-built dimensions for dimensional compliance control in construction.” Advanced Engineering Informatics, 24(1), 107-118.

Bosche, F. and Haas, C.T. (2007). “Towards automated comparison of 3D sensed and 3D designed data.” International Workshop on Computing in Civil Engineering, Pittsburgh, PA, USA, 548-556.

Bosche, F. and Haas, C.T. (2008). “Automated retrieval of 3D CAD model objects in construction range images.” Automation in Construction, 17(4), 499-512.

Bosche, F., Haas, C.T., and Akinci, B. (2009). “Automated Recognition of 3D CAD Objects in Site Laser Scans for Project 3D Status Visualization and Performance Control.” Journal of Computing in Civil Engineering, 23 (6) 311–318.

Bouguet, J. (2010). “Camera Calibration Toolbox for Matlab.” <http://www.vision.caltech.edu/bouguetj/calib_doc/>, (Jul. 9, 2010).

Brass, L. (2007). “A Glimpse of the Energy Future,” Oak Ridge National Laboratory Review, 40(2), 2-7.

Brilakis, I., and Soibelman, L. (2008). “Shape-based retrieval of construction site Photographs.” Journal of Computing in Civil Engineering, 22(1), 14 – 20.

Brilakis, I., Lourakis, M., Sacks, R., Savarese, S., Christodoulou, S., Teizer, J., and Makhmalbaf. A. (2010). “Toward automated generation of parametric BIMs based on hybrid video and laser scanning data.” Adv. Eng. Inform. 24(4), 456-465.

Cheok, G.S., Stone, W.C., Lipman, R.R., and Witzgall, C. (2000) “Ladars for construction assessment and update.” Automation in Construction, 9(5-6), 463-477.

Cho, Y., and Martinez, D. (2009). "Light-weight 3D LADAR System for Construction Robotic Operations." 26th International Symposium on Automation and Robotics in Construction (ISARC), Austin, Texas, June 24-27, 237-244.

Cho, Y., Haas, C., Liapi, K., and Sreenivasan, S. (2002). “A framework for rapid local area modeling for construction automation.” Automation in Construction, 11 (6) 629–641.

Cho, Y., Wang, C., Tang, P., and Haas, C. (2012). “Target-focused Local Workspace Modeling for Construction Automation Applications.” Journal of Computing in Civil Engineering, ASCE, 26(5), 661-670.

ClearEdge3D. (2014). <http://www.clearedge3d.com/ >, (Jan. 27, 2014).

Dai, F. and Lu, M. (2010). “Assessing the Accuracy of Applying Photogrammetry to Take Geometric Measurements on Building Products.” J. Constr. Engr. and Mgmt., 136(2), 242-250.

DirectIndustry (2010). <http://www.directindustry.com/industrial-manufacturer/handheld-laser-scanner-75269.html> (Jan. 3, 2010).

Drennan, M. (2010). “An Implementation of Camera Calibration Algorithms.” <http://www.ces.clemson.edu/~stb/ece847/projects/Camera_Calibration.pdf>. (May 25, 2011)

El-Omari, S. and Moselhi, O. (2008). “Integrating 3D laser scanning and photogrammetry for progress measurement of construction work.” Journal of Automation in Construction, 18(1), 1-9.

Energy Information Agency (EIA), (2009). “Annual Energy Review 2008.” DOE/EIA-0384 (2008), U.S. Department of Energy, June 2009.

Farid, R. and Sammut, C. (2012). “A Relational Approach to Plane-based Object Categorization.” RSS 2012 Workshop on RGB-D Cameras, Jul. 2012. [Online]. Available: http://www.cs.washington.edu/ai/Mobile Robotics/rgbd-workshop-2012/ papers/farid-rgbd12-object-categorization.pdf

Farid, R. and Sammut, C. (2013). “Plane-based object categorization using relational learning.” Machine Learning, 1-21.

FARO Technology Ltd (2010). “FARO Focus 3D Data Sheet.” http://www.ats.se/data/FocUsTechSheet.pdf (March 9, 2011)

Golparvar-Fard, M. and Peña-Mora, F. (2007). “Application of visualization techniques for construction progress monitoring.” Proceedings of the ASCE International Workshop on Computing in Civil Engineering, Pittsburgh, PA, 261(27), 216-223.

Golparvar-Fard, M., Bohn, J., Teizer, J., Savarese, S., and Peña-Mora, F. (2011). “Evaluation of image-based modeling and laser scanning accuracy for emerging automated performance monitoring techniques.” Automation in Construction, 20, 1143–1155.

Golparvar-Fard, M., Peña-Mora, F., Arboleda, C., and Lee, S. (2009a). “Visualization of construction progress monitoring with 4D simulation model overlaid on time-lapsed photographs.” ASCE Journal of Computing in Civil Eng., Special Ed. on Graphical 3D Visualization in Architecture, Engineering, and Construction, 391–404.

Golparvar-Fard, M., Peña-Mora, F., and Savarese, S. (2009b). “D4AR- A 4-Dimensional augmented reality model for automating construction progress data collection, processing and communication.” Journal of Information Technology in Construction (ITcon), Special Issue Next Generation Construction IT: Technology Foresight, Future Studies, Roadmapping, and Scenario Planning 14, 129-153, http://www.itcon.org/2009/13.

Gordon, C. and Akinci, B. (2005). “Technology and process assessment of using LADAR and embedded sensing for construction quality control.” Construction Research Congress, San Diego, CA, USA

Gordon, S. J., Lichti, D.D., Stewart, M.P., and Franke, J. (2004). “Modeling point clouds for precise structural deformation measurement.” Proceedings of the XXth ISPRS Congress, Istanbul, Turkey, 954-959.

Ham, Y., and Golparvar-Fard, M. (2012). “Rapid 3D Energy Performance Modeling of Existing Buildings using Thermal and Digital Imagery.” Proceedings of Construction Research Congress 2012, ASCE, West Lafayette, IN, 991-1000.

Hegde, G. M. and Ye C. (2008) “SwissRanger SR-3000 range images enhancement by a singular value decomposition filter.” Information and Automation, 2008. ICIA 2008. International Conference on , 20-23.

doi: 10.1109/ICINFA.2008.4608264

Heikkila, J., and Silven, O. (1997). “A Four-step Camera Calibration Procedure with Implicit Image Correction.” IEEE Computer Society Conference on Computer Vision and Pattern Recognition, IEEE, San Juan, Puerto Rico, 1106-1112.

Heinz, I., Hartl, F., and Frohlich, C. (2001). “Semi-automatic 3D CAD model generation of as-built conditions of real environments using a visual laser radar.” Robot and Human Interactive Communication. Proceedings. 10th IEEE International Workshop on, 400-406.

Hill, F. S., and Kelley, S. M. (2006). “Rendering Faces for Visual Realism.” Computer graphics: using OpenGL, Pearson Prentice Hall, Upper Saddle River, NJ.

Im, H., Gai, M., Wang, C., and Cho, Y. (2012). “Hybrid Approach to Visualize Building Energy Information Model in Geospatial Application Programs.” Proceedings of Construction Research Congress 2012, ASCE, West Lafayette, IN, 1262-1270.

Intergraph. (2014). <http://www.intergraph.com/products/ppm/smart_3d/plant/default.aspx>, (Jan. 27, 2014).

Jaselskis, E.J., Cackler, E.T., Walters, R.C., Zhang, J., and Kaewmoracharoen, M. (2006). “Using scanning lasers for real-time pavement thickness measurement.” CTRE Project 05-205, Iowa State University. Ames, IA, USA.

Jaselskis, E.J., Gao, Z., and Walters, R.C. (2005). “Improving transportation projects using laser scanning.” Journal of Construction Engineering and Management 131(3) 377-384.

Kemeny, J., and Turner, K. (2008). “Ground-based LiDAR Rock slope Mapping and Assessment.” Technical Report FHWA-CFL/TD-08-006, Central Federal Lands Highway Division, Lakewood, CO.

Kim, C., Son, H., and Kim, C. (2013). “Fully Automated Registration of 3D Data to a 3D CAD Model for Project Progress Monitoring.” Auto. Constr., 35, 587-594.

Kim, C., Haas, C.T., and Liapi, K.A. (2005). “Rapid, on-site spatial information acquisition and its use for infrastructure operation and maintenance, Automation in Construction, 14 (5), 666-684.

Kleder, M. (2005). “Covert lat, lon, alt to ECEF Cartesian,” <http://www.mathworks.com/matlabcentral/fileexchange/7942-covert-lat-lon-alt-to-ecef-cartesian>.

Kleder, M. (2006).“Convert Cartesian (ECEF) Coordinates to lat, lon, alt,” <http://www.mathworks.com/matlabcentral/fileexchange/7941-convert-cartesian-ecef-coordinates-to-lat-lon-alt>.

Kubit. (2014). <http://us.kubit-software.com/CAD/Products/PointSense/index.php>, (Jan. 27, 2014).

Kwon, S.W., Bosche, F., Kim, C., Haas, C. T. and Liapi, K. A. (2004). “Fitting range data to primitives for rapid local 3D modelling using sparse range point clouds.” Automation in Construction, 13(1), 67-81.

Lagüela, S., Armesto, J., González-Jorge, H., Arias, P., and Herráez, J. (2011a). “Automation of Thermographic 3D Modelling through Image Fusion and Image Matching Techniques.” Proceedings of 28th International Symposium On Automation and Robotics In Construction (Part II), IAARC, Seoul, Korea, 212-227.

Lagüela, S., Martínez, J., Armesto, J., and Arias, P. (2011b). “Energy Efficiency Studies through 3D Laser Scanning and Thermographic Technologies.” Energy and Buildings, 43(6), 1216-1221.

Leica Geosystems. (2014). < http://www.leica-geosystems.us/en/Leica-CloudWorx_60696.htm>, (Jan. 27, 2014).

Linder, W. (2003). “Digital Photogrammetry.” Springer-Verlag, New York, Inc..

Luhmann, T., Robson, S., Kyle, S., and Harley, I. (2006)."Close Range Photogrammetry. Principles, Methods and Application", Whittles Publishing, Caithnesss, UK.

Ma, L., Chen, Y., and Moore, K. L. (2003). “A New Analytical Radial Distortion Model for Camera Calibration.” IEEE Computer Society Conference on Computer Vision and Pattern Recognition, IEEE, Madison, WI.

Maldague, X. P. V. (2001). “Theory and Practice of Infrared Technology for Nondestructive Testing.” Wiley-Interscience.

Mesa Imaging (2010). “SR4000 Data Sheet.” < http://www.mesa-imaging.ch/Prodview4k.php> (Dec. 8, 2010).

Moravec, H. (1996). “Robot Spatial Perception by Stereoscopic Vision and 3D Evidence Grids.”

National Renewable Energy Laboratory (NREL) (2008). “Building America Research Benchmark Definition.” Technical Report NREL/TP-550-44816.

Navon, R. (2007). “Research in automated measurement of project performance indicators.” Automation in Construction, 16(2), 176–188.

Nüchter, A. (2012). Project ThermalMapper, <http://www.faculty.jacobs-university.de/anuechter/thermalmapper.html>, (Nov 1, 2011).

Ocaña, M. S., Guerrero, C. I., and Requena, G. I. (2004). “Thermographic survey of two rural buildings in Spain.” Energy and Buildings, 36(6), 515–523.

Olson, D.L. and Delen, D. (2008). “Advanced Data Mining Techniques.” Springer, 1st edition, page 138, ISBN 3540769161.

Pu, S. and Vosselman, G. (2009). “Knowledge based reconstruction of building models from terrestrial laser scanning data.” ISPRS Journal of Photogrammetry and Remote Sensing, 64, 575-584.

Rao, D. S. (2007). “Investigations on Ancient Masonry Structures Using Infrared Thermography.” Proc. of InfraMation 2007 Conference, Las Vegas, NV.

Rebolj, D., Babic, N.C., Magdic, A., Podbreznik, P., and Psunder, M. (2008). “Automated construction activity monitoring system, Advanced Engineering Informatics, 22(4), 493-503.

Rosina, E., and Spodek, J. (2003). “Using infrared thermography to detect moisture in historic masonry: a case study in Indiana.” APT Bulletin, 34, 11–16.

Rusu, R., Blodow, N., Marton, Z., Soos, A., and Beetz, M. (2007). “Towards 3D Object Maps for Autonomous Household Robots.” International Conference on Intelligent Robots and Systems, IEEE, San Diego, CA, Oct. 29 - Nov. 2.

Schreyer, A. C., and Hoque, S. (2009). “Interactive Three-Dimensional Visualization of Building Envelope Systems Using Infrared Thermography and SketchUp.” Proc. of InfraMation 2009, Las Vegas, NV.

Smithm, J. (2011). “Handheld 3D Scanner-Affordable and Easy Form of 3D Scanning System.” Ezine Articles, <http://ezinearticles.com/?Handheld-3D-Scanner---Affordable-and-Easy-Form-of-3D-Scanning-System&id=1460968> (Jan.3, 2011)

Son, H., and Kim, C. (2010). “3D structural component recognition and modeling method using color and 3D data for construction progress monitoring.” Automation in Construction, 19, 844-854.

Stone, W.C., Juberts, M., Dagalakis, N., Stone, J., and Gorman, J. (2004). “Performance analysis of next-generation LADAR for manufacturing, construction, and mobility.” NIST Interagency/Internal Report (NISTIR) - 7117, Gaithersburg, Md.

Tang, P. and Akinci, B. (2012). “Automatic execution of workflows on laser-scanned data for extracting bridge surveying goals.” Advanced Engineering Informatics, 26(4), 889-903.

Tang, P., Akinci, B., and Huber, D. (2009). “Quantification of edge loss of laser scanned data at spatial discontinuities.” Autom. Constr., 18(8), 1070-1083.

Tang, P., Akinci, B., James, H., and Garrett, J. (2007). Laser "Scanning for Bridge Inspection and Management." IABSE Symposium, Weimar, Germany. 206-207.

Tang, P., and Akinci, B. (2008). "Automated measurement extraction from laser scanned point clouds to support bridge inspection." IABSE Symposium, Weimar, Germany.

Tang, P., Huber, D., Akinci, B., Lipman, R., and Lytle, A. (2010). "Automatic reconstruction of as-built building information models from laser-scanned point clouds: A review of related techniques." Automation in Construction, 19(7), 14.

Tang, P., Huber, D., and Akinci, B. (2011). "Quantification of edge loss of laser scanned data at spatial discontinuities." Journal of Computing in Civil Engineering 25(1) 31-42.

Trimble. (2014). < http://www.trimble.com/3d-laser-scanning/realworks.aspx?dtID=overview& >, (Jan. 27, 2014).

Tsai, F., and Lin, H. (2004). "Realistic Texture Mapping on 3D Building Models." http://www.a-a-r-s.org/acrs/proceeding/ACRS2004/Papers/3DG04-6.htm (12/23/2010).

U.S. Department of Energy. (2011). "2011 U.S. DOE buildings energy databook." <http://buildingsdatabook.eren.doe.gov/>, (Apr. 15, 2012).

Wu, Y. and Kim, H. (2004). "Digital imaging in assessment of construction project progress." Proc. Of the 21th ISARC, 537 – 542.

Xiong, X., Adan, A. Akinci, B., and Huber, D. (2013). "Automatic creation of semantically rich 3D building models from laser scanner data." Automation in Construction, 31, 325-337.

Z Corporation (2011). ZScanner, <http://zscanner.com/en/Products/3D-Scanners/ZScannerandtRade-700/Self-Positioning/spage.aspx> (Jan.3, 2011).

Zhou, P. (2005). "Computational Geometry: Analysis and Design on the Algorithms." second edition, Tsinghua University press, Beijing.

# VITA

## CHAO WANG

Chao Wang was born in Yantai, China. He received a Bachelor's degree in Electrical Engineering from Hohai University, China in 2006, and a Master's degree in Transportation Engineering from Beihang University, China in 2009. From August 2009, Chao started to pursue a doctoral degree in Construction at University of Nebraska-Lincoln, and transferred to the Civil Engineering program at Georgia Institute of Technology in August 2013. Chao has worked on several projects funded by state or federal agencies during his doctoral study. He also worked as a teaching assistant and lab instructor for several construction courses including construction equipment and methods, building information modeling, construction graphics and design process, virtual design and construction, and construction engineering and management. His current research areas include construction robotics, remote sensing, data visualization, data acquisition system design, real-time monitoring of the built environment, as-is BIM modeling, and pavement quality control and assurance. Chao's research aims to enhance construction safety and efficiency by utilizing emerging data sensing technology. By the time of his graduation, Chao's research findings will have been presented in multiple journal publications and conference proceedings.